geomatics

MDPI

Article

Geospatial Scenario Modeling with Cellular Automata: Land Use and Cover Change in Southern Maranhão, Brazilian Savanna (2020–2030)

Paulo Roberto Mendes Pereira [1,2,*], Édson Luis Bolfe [1,3,*], Francisco Wendell Dias Costa [4], Taíssa Caroline Silva Rodrigues [5], Marcelino Silva Farias Filho [2] and Eduarda Vaz Braga [5]

1 Graduate Programme in Geography, State University of Campinas, Campinas 13083-876, SP, Brazil
2 Graduate Programme in Geography, Federal University of Maranhão, São Luiz 65085-580, MA, Brazil; marcelino.farias@ufma.br
3 Embrapa Digital Agriculture, Brazilian Agricultural Research Corporation, Campinas 13083-970, SP, Brazil
4 Federal Institute of Maranhão, Barra do Corda 659500-00, MA, Brazil; francisco.dias@ifma.edu.br
5 Graduate Programme in Environmental Sciences, State University of the Tocantina Region of Maranhão, Imperatriz 65901-480, MA, Brazil; taissa.rodrigues@uemasul.edu.br (T.C.S.R.); eduardabraga.20200003458@uemasul.edu.br (E.V.B.)
* Correspondence: p229468@dac.unicamp.br (P.R.M.P.); ebolfe@ige.unicamp.br (É.L.B.)

Abstract

Land use and land cover (LULC) changes driven by agricultural and livestock expansion pose significant threats to the Brazilian savanna (Cerrado). This study aimed to analyze, map, and simulate LULC changes in the southern mesoregion of Maranhão State by generating geospatial scenarios projected through 2030. LULC changes between 2015 and 2020 were analyzed using Landsat images classified with the Random Forest machine learning algorithm. A spatial model based on cellular automata was employed to simulate land use and land cover scenarios for the year 2030. When comparing the simulated map with the reference map, an overall accuracy of 70.28% and a Kappa index of 0.608 were observed. Results revealed a decrease in native savanna and grassland areas, with a corresponding increase in agricultural and pasturelands, notably in municipalities such as Balsas, Riachão, Tasso Fragoso, Carolina and Porto Franco. The 2030 simulation predicts continued agricultural expansion and a potential reduction of approximately 19% in native Cerrado vegetation cover, highlighting municipalities of Campestre do Maranhão, Porto Franco, São João do Paraíso, Feira Nova, Estreito, Balsas, Tasso Fragoso and Carolina. These findings underscore the value of integrating remote sensing and spatial modeling techniques within the framework of Geomatics to support environmental monitoring and management of land-use dynamics, including expansion, contraction, diversification, and agricultural intensification. This approach provides critical insights into anthropogenic impacts on sensitive ecosystems, informing sustainable planning in tropical savanna regions.

Keywords: remote sensing; machine learning; GIS; Landsat; Cerrado; Brazil

Academic Editor: Giorgos Mallinis

Received: 28 August 2025
Revised: 29 October 2025
Accepted: 8 November 2025
Published: 17 November 2025

Citation: Pereira, P.R.M.; Bolfe, É.L.; Costa, F.W.D.; Rodrigues, T.C.S.; Farias Filho, M.S.; Braga, E.V. Geospatial Scenario Modeling with Cellular Automata: Land Use and Cover Change in Southern Maranhão, Brazilian Savanna (2020–2030). *Geomatics* **2025**, *5*, 65. https://doi.org/10.3390/geomatics5040065

1. Introduction

Land use and land cover (LULC) changes are considered one of the main consequences of human activities on geographic space, especially due to the rapid pace at which they occur and the associated biophysical, political, social, and economic impacts. These processes can not only affect local areas but also extend to regional and global scales [1–3]. One of the most effective ways to analyze and identify land use and land cover changes is

through the classification of remote sensing imagery—an important tool for monitoring transformations on the Earth's surface. This method allows for systematic and reliable detection of major spatial changes over time, particularly in large territorial environments, and at a relatively low cost.

Another significant application of land cover information is the use of dynamic models to create scenarios of land use and cover. This cartographic technique focuses on representing dynamic processes and identifying potential impacts, whether associated with anthropogenic activities or not. It aids in implementing environmental policies, guiding decision-making, and mitigating potential negative consequences of human actions. Highlights that these models are primarily based on the concept of cellular automata, which involves a simulation framework where space is represented as a grid of cells, and a set of transition rules determines each cell's attributes, taking into account the attributes of its neighboring cells [4].

A dynamic model is defined as a representation of real-world processes or phenomena that seeks to overcome the limitations of static, two-dimensional representations by incorporating spatial patterns that change over time [5]. Dynamic modeling aims to understand the causal mechanisms driving the development of various systems, thereby enabling the prediction of their likely evolution, the testing of hypotheses, and the exploration of potential trajectories of spatial change [6]. Dynamic spatial models describe the evolution of a system's spatial patterns over time and must address the following questions [7,8]: Which environmental and cultural variables contribute to explaining the phenomenon? What are the underlying ecological and socio-economic processes driving the phenomenon? How does the process evolve? Where do these phenomena occur? These key questions align with the classical "Why," "When," and "Where." A model capable of answering these questions can quantitatively describe a phenomenon and predict its evolution, integrating its temporal and spatial scales.

It is essential to emphasize that LULC dynamic models do not possess the ability to predict the future. Instead, they provide, with a certain level of confidence, indications of a phenomenon's behavior based on predefined parameters, characteristics, or known patterns. Generally, these models consider various factors to simulate the dynamics of change, enabling the establishment of measures for land-use planning [9–13].

The Cerrado, Brazil's second-largest biome, accounts for 35% of the country's territory, covering approximately 200 million hectares and spanning the boundaries of 10 states. It is considered strategic from ecological, economic, social, and cultural perspectives, primarily due to its environmental characteristics, biodiversity, and ecosystem services. The biome contains more than 5% of global biodiversity, featuring a rich flora with over 12,000 plant species, as well as a wide variety of mammals and insects. Another critical characteristic of the Cerrado is its high capacity for hydrological regulation and maintenance, hosting key recharge areas for significant Brazilian river basins [14].

Despite its importance in maintaining water resources and biodiversity, only 13.29% of the Cerrado's area is protected by conservation units, Indigenous lands, or quilombola territories, with merely 5.7% of the biome being fully protected by these mechanisms [13,14]. This limited protection has directly contributed to the high rates of native vegetation loss, driven mainly by the rapid expansion of agricultural frontiers [15–17].

According to mappings by [16], approximately 45% of this biome has been anthropized, a consequence of the rapid advance of the modern agricultural frontier into the central portion of the country, a factor that has placed the Cerrado on the list of global biodiversity conservation hotspots. Currently, this advance is occurring in the states that comprise the MATOPIBA region [18,19]. Considered the last frontier of modern national agribusiness expansion, with an area of approximately 73.0 million hectares—35% of the total Cerrado

territory—it includes municipalities in Maranhão, Tocantins, Piauí, and Bahia, responsible for a significant share of national commodity production [19–22].

In the state of Maranhão, the Cerrado biome covers an area of 212,518 km^2 distributed across 119 municipalities, and has shown high rates of natural vegetation conversion, primarily for agriculture and livestock [12,13]. Between 2015 and 2020 alone, the state lost approximately 835,000 hectares of Cerrado vegetation, with the Southern Maranhão Mesoregion taking a leading role. Covering an area of approximately 67,600 km^2—31% of the entire Cerrado in Maranhão—this region is characterized as the state's main agricultural production hub, accounting for about 30% of Maranhão's Gross Domestic Product (GDP). It is also recognized as one of the principal areas for agricultural commodity production both nationally and globally [13,23].

Although initiated in the 1960s, the process of modern agribusiness expansion in the area is considered recent, gaining intensity from the 1990s. During this period, municipalities within the region, particularly Balsas, became part of what can be referred to as "programs and policies for the expansion and modernization of Brazilian agriculture" [24,25]. Notably, PRODECER III and the North–South Export Corridor (later designated as the North Export Corridor) were fundamental in consolidating Southern Maranhão within the global agricultural commodity production network. This shift resulted in profound transformations in the area's productive structure, which was previously based on livestock and small-scale farming, primarily rice cultivation. It transitioned to a highly mechanized production system, predominantly featuring soybean monoculture, along with corn, sugarcane, and cotton [26–28].

As a result, the area has undergone significant transformations in land cover and use, primarily due to the high rate of natural vegetation loss. The municipalities within the Southern Maranhão Mesoregion accounted for approximately 7.11% of the total deforested area in the Cerrado biome between 2015 and 2022. During this period, approximately 650,000 hectares of vegetation were converted to anthropic land classes, positioning the region among the leaders in vegetation loss. Notably, the municipality of Balsas has led the list of natural vegetation loss in the Cerrado since 2020 [29]. On the other hand, the area still holds a vast amount of land with natural vegetation legally available for conversion, placing it at the center of discussions on environmental conservation, economic development, and natural resource protection [30–32].

The presence of unconverted areas in the region can be a decisive factor in agricultural expansion, particularly because they retain a significant coverage of native vegetation. Another important point is that, unlike the Amazon, where legal protection reaches 80%, the Cerrado's Legal Reserve requirement is only 35%, according to the Forest Code (Law No. 12.651/2012). This makes the Cerrado more vulnerable to land conversion, as it increases the availability of areas legally suitable for agricultural use. Furthermore, the emergence of production incentive public programs and policies favoring agribusiness exert additional pressure on these remaining areas, reinforcing the perception of the region as a strategic agricultural frontier. Thus, the combination of lower legal protection and the presence of unconverted areas promote agricultural expansion, while simultaneously jeopardizing the conservation of the biome's biodiversity and ecosystem services.

Given the above, simulating trends in the loss of natural Cerrado vegetation is of paramount importance for the geoenvironmental planning of this region, as it corresponds to a priority area for conservation [31,33], primarily due to its importance in maintaining biodiversity, ecosystem services, and water resources in the state of Maranhão [13,17,18]. From this perspective, this study aims to simulate future land use and land cover scenarios for the Southern Maranhão Mesoregion by projecting observed changes between 2015 (t1) and 2020 (t2). The study specifically focuses on analyzing landscape dynamics in

municipalities affected by the expansion of mechanized agriculture within the Maranhão Cerrado, a region exhibiting high susceptibility to desertification processes, particularly in the eastern and southern mesoregions [34]. Using a combination of remote sensing, Random Forest classification, and cellular automata-based spatial modeling, this research offers a novel methodological approach to quantifying and predicting land use and land cover transformations. The outcomes provide detailed insights into the spatial patterns and trends of natural Cerrado vegetation loss, supporting targeted land management strategies and informing policy decisions (public and private) aimed at sustainable resource use in the region of the Maranhão state, Brazil.

2. Materials and Methods

2.1. Study Area Location

The study area comprises the Southern Maranhão Mesoregion (Figure 1), located in the southern portion of the state of Maranhão. It covers approximately 67,693.40 km^2 and consists of the municipalities of Alto Parnaíba, Balsas, Benedito Leite, Campestre do Maranhão, Carolina, Estreito, Feira Nova do Maranhão, Fortaleza dos Nogueiras, Loreto, Nova Colinas, Porto Franco, Riachão, Sambaíba, São Domingos do Azeitão, São Félix de Balsas, São João do Paraíso, São Pedro dos Crentes, São Raimundo das Mangabeiras, and Tasso Fragoso.

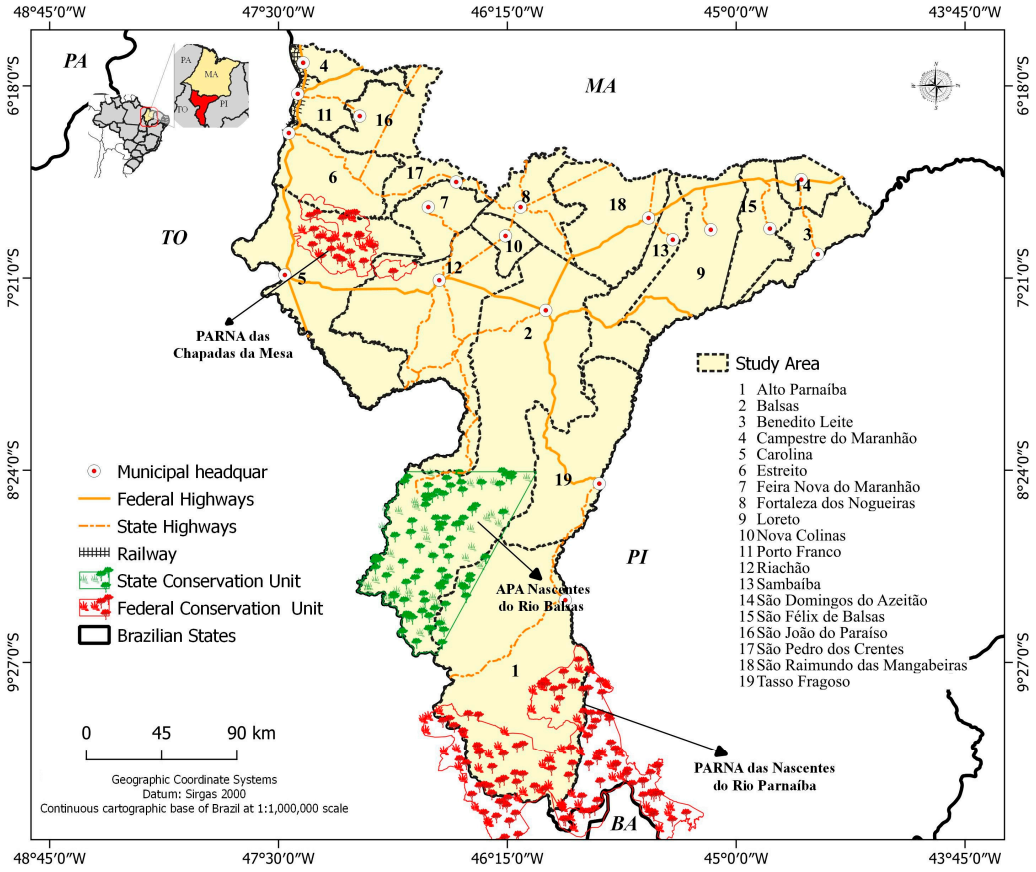

Figure 1. Location of the Southern Maranhão State Mesoregion, Brazil. Source: the authors.

The area is bounded to the west and south by the municipalities of Aguiarnópolis, Babaçulândia, Barra do Ouro, Campos Lindos, Darcinópolis, Filadélfia, Goiatins, Lizarda, Mateiros, and Palmeiras do Tocantins, belonging to the state of Tocantins; to the east by the state of Piauí; and to the north by the Northern Maranhão, Central Maranhão, and Eastern Maranhão mesoregions. With a total population of 332,539 inhabitants, it has a low

population density of 5 inhabitants/km^2, where 87% of the population resides in urban areas. The main economic activity is mechanized agriculture for soybean production, with the municipality of Balsas as the regional economic hub.

Balsas alone accounts for 3.5% of the GDP of the state of Maranhão and concentrates the provision of key financial, logistical, industrial, and commercial services. This scenario is closely linked to the agricultural production dynamics of Balsas, which, along with neighboring municipalities such as Tasso Fragoso, Riachão, and São Raimundo das Mangabeiras, has the largest agricultural production area in the state, a factor that also fosters the development of other economic activities directly related to the agricultural sector.

The choice of this area was based on its regional and national relevance, as it represents the last frontier of agricultural expansion in the Brazilian Cerrado. The region still has a significant amount of land available for cultivation and plays a fundamental role in biodiversity conservation [33,34]. Moreover, its social, economic, and environmental importance transcends national boundaries, since these savanna areas harbor a considerable share of global biodiversity. From a scientific perspective, this context reinforces the need for studies that assess the degree of Cerrado degradation and its potential future impacts.

Regarding the characteristics that shape the local landscape, it has a predominantly sedimentary geological foundation, composed of partially silicified sandstones with layers of siltstones and shales, flint, and other more durable cementing compounds, interspersed with limestone and more erosion-prone sandstones, as well as petromictic conglomerates. These are overlaid on sequences of sandstones of varying grain sizes, limestones, siltstones, conglomerates, shales, schists, and argillites [35]. In terms of altimetric conditions, the Southern Maranhão Mesoregion presents an altimetric range of 684 m, with an average elevation of 368 m. The lowest altitudes are around 123 m, while the highest reach 814 m. The topography is predominantly flat, interspersed with a set of steep residual tabular features—mesas, plateaus, and tablelands—and low hills, generally with flat tops and varying altitudes. These are overlaid by wide, entrenched valleys, with notable areas of depressions and broad fluvial plains of the Balsas, Tocantins, Parnaíba, and other rivers [35].

The soils of the microregion within the Southern Maranhão Mesoregion are associated with sedimentary lithology, predominantly comprising Latosols and Neosols, with lesser proportions of Argisols, Nitisols, Plinthosols, Gleisols, and Luvissols [35]. The prevailing climate is tropical subhumid, characterized by two well-defined seasons: a dry season from July to September and a rainy season from October to March. Precipitation ranges from moderate to high, with annual totals between 800 and 1600 mm, a summer potential evapotranspiration rate of 24.6%, and relative humidity above 70%. The region experiences a water deficit of 467 mm from July to December, followed by water replenishment starting in January, with a surplus of 660 mm concentrated between October and March [36].

The interaction between climatic, geological, pedological, and topographic factors conditions the development of vegetation typical of the Cerrado biome. This vegetation is characterized by trees with twisted trunks and stems, large leaves adapted to climatic seasonality, and soils that are generally poor, deep, and rich in aluminum. The vegetation also exhibits significant adaptation to the natural fire dynamics to which the region is subjected [35,36]. The biome is classified into three distinct phytophysiognomies: (i) forest formations, (ii) savanna formations, and (iii) grassland formations.

2.2. Methodological Procedures

Figure 2 presents the methodological flowchart for agricultural expansion scenario modeling, which was conducted in two stages. All spatial datasets used in this study were referenced to the SIRGAS 2000 geodetic datum and expressed in geographic coordinates (latitude and longitude), ensuring consistency across all geoprocessing stages.

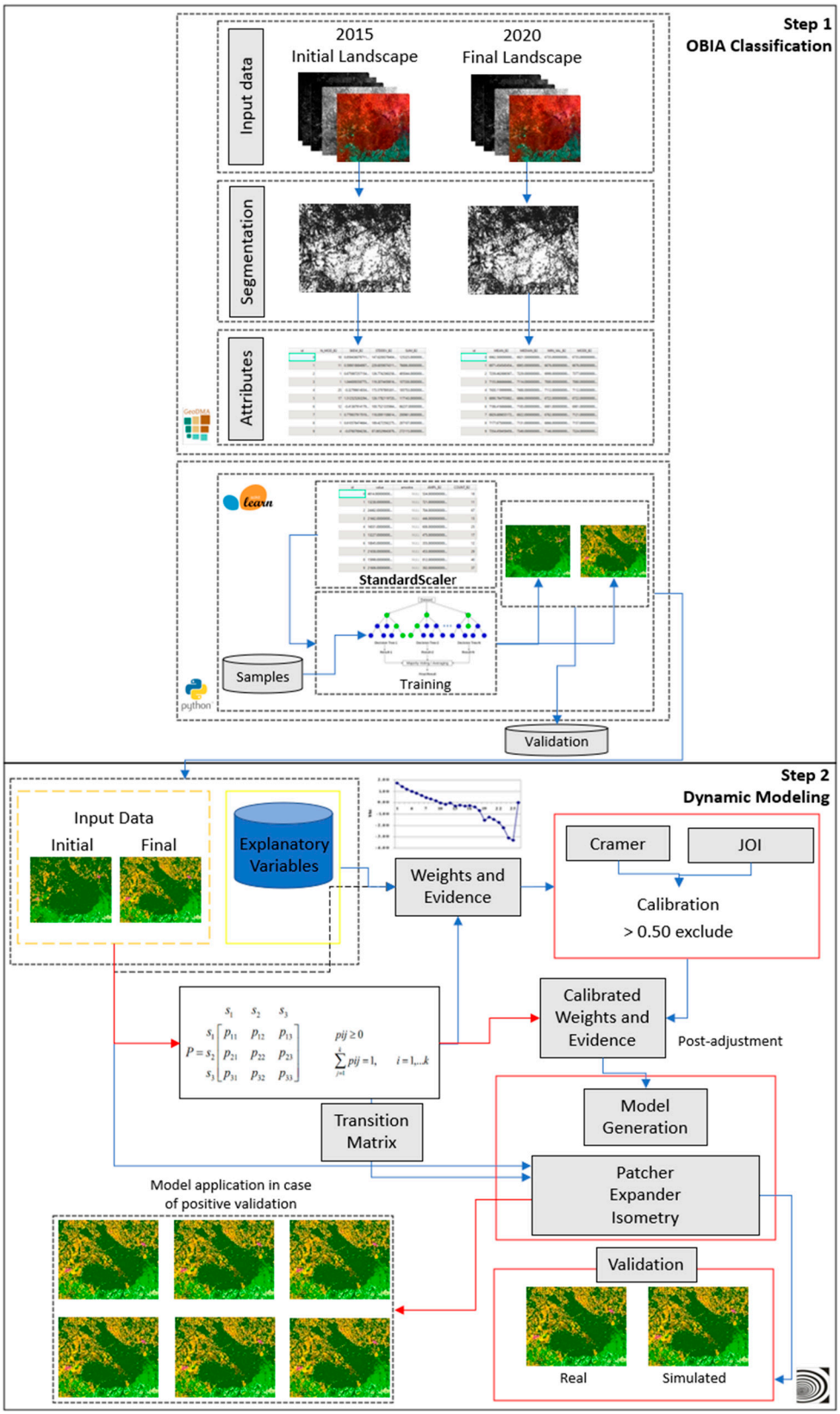

Figure 2. Methodological framework showing the phases in this study. Source: the authors.

In the first stage, a classification process was carried out for land use and cover mapping using Object-Based Image Analysis (OBIA) techniques [37], divided into the following steps: (a) segmentation, (b) attribute extraction, (c) classification, and (d) statistical

validation. The second stage involved generating scenarios of natural Cerrado vegetation loss in the area through 2030, using cellular automata combined with the weights of evidence method.

The correlation between statistical variables is analyzed. Since the weights-of-evidence method is based on the conditional probability of the occurrence or non-occurrence of a transition, the variables must be independent, making it necessary to remove those with high correlation. In "Dinâmica EGO" [6,38], Cramér's V and Joint Information Uncertainty (JIU or U) indices are used. These indices assess the spatial dependence between two variables in relation to a specific type of transition [39]. While Cramér's V measures the degree of association using actual area values, providing a more rigorous analysis, the JIU operates with percentage values of the transition area between different classes.

This was implemented on the environmental modeling platform "Dinâmica EGO" (Environment for Geoprocessing Objects) [6,38] a free, open-source, non-commercial platform developed in C++ with a graphical interface in Java. Its graphical interface is based on a patented data flow system maintained by the Remote Sensing Center (CSR) at the Geosciences Institute of the Federal University of Minas Gerais (UFMG) [6].

2.2.1. Data Used

Landsat 8 images were used, covering the orbits/paths 220/65, 221/65, 221/66, and 221/67 for the years 2015 and 2020, with a spatial resolution of 30 m, collection 2 level 2, provided already calibrated, with geometric and radiometric corrections and surface reflectance data supplied by the United States Geological Survey (USGS) image catalog (https://www.usgs.gov/landsat-missions/landsat-data-access, accessed 15 July 2024).

The selection of satellite images considered the percentage of cloud cover, with images containing a maximum of 5% cloud cover being chosen [40,41]. To enhance the separability of targets, a set of spectral indices derived from the images was calculated, including NDVI [42], SAVI and EVI [42], NDWI [43], and NDBI [44]. All the data were merged into a single file containing all the layers of information.

2.2.2. Land Use and Land Cover Mapping

The first stage consists of the digital image classification process. Initially, the set of images was segmented, which corresponds to the grouping of pixels with similar characteristics—such as specific ranges of intensity, texture, or color—forming discrete, contiguous, and non-overlapping regions. These regions semantically aim to change the image representation regression and classification algorithm that creates and fits an ensemble of decision tree classifiers, which, when combined, provide high accuracy [45]. For this purpose, a series of routines were developed in the Python programming environment, based on the use of the Scikit-Learn machine learning library, where the RF tuning parameters are implemented—these being the number of variables per leaf (mtry) and the maximum number of trees (ntree) [46–49].

To train the classifier, a series of sample points were collected, using both imagery by fragmenting it into areas that may or may not correspond to objects [46,50]. The region-growing algorithm was used, which aggregates pixels starting from a "seed" pixel and progressively groups pixels with similar properties based on similarity values and scale [47]. The choice of region-growing segmentation was primarily driven by its ease of implementation within a GIS environment. In the CR segmentation algorithm, it is important to note that the similarity and scale thresholds do not follow a pre-established rule; rather, they are determined empirically through iterative testing until the optimal visual pattern is achieved. This approach allows for the semantic separation of distinct objects according to the analyst's criteria.

To optimize the segmentation, multiple tests were conducted varying both area size and similarity parameters. A similarity threshold of 0.010 and a minimum area of 12 pixels were selected for all image sets, corresponding to approximately one hectare. These settings provided the most accurate representation of objects in images with a 30 m spatial resolution, ensuring that the segmentation captured meaningful landscape features while minimizing over- or under-segmentation. After the segmentation step, a series of attributes were calculated, totaling eight statistical indices (mean, standard deviation, variance, kurtosis, maximum, minimum, median, and skewness) for each of the information layers, resulting in 77 attributes. To remove magnitude differences and thus avoid data bias, this process was carried out in a Python 3.10 programming environment using the StandardScaler algorithm from the preprocessing package implemented in the Scikit-Learn library.

To reduce the dimensionality of the dataset, a Principal Component Analysis (PCA) was applied. This multivariate statistical technique identifies orthogonal directions of maximum variance, allowing the data to be represented in a lower-dimensional space without substantial loss of information [50,51]. The PCA was implemented in Python using the scikit-learn library. A total of 10 principal components were retained, explaining 98% of the total variance, thereby ensuring that most of the original information was preserved for subsequent classification steps. The mean NDWI showed the highest loading on the first component, followed by the mean NDVI, which together accounted for approximately 78% of the explained variance among the selected components.

The segments were classified using the Random Forest (RF) classifier, non-parametric and supervised and field-collected points as reference. The following classes were identified: forest formations, savanna formations, grassland formations, pastures, agriculture, temporary crops, silviculture, and water. The sample size considered the coverage pattern of each thematic class, recognizing that this parameter is not homogeneous.

Field activities for collecting data to support classification and validation were carried out in 2021 and 2023, where information on the main vegetation cover types and land uses was collected (Figure 3). The number of samples and their spatial distribution per class used for classifier training varied. In 2015, a total of 2310 points were collected, distributed as follows: 380 forest formations, 407 savanna formations, 332 grassland formations, 494 pastures, 458 agriculture – crops, 172 silviculture, 94 exposed soil points, and 73 water points. For 2020, 2400 points were used, consisting of 381 forest formations, 407 savanna formations, 325 grassland formations, 417 pastures, 518 temporary crops, 183 silviculture, 90 exposed soil points, and 79 water points. For classification, a random balancing procedure was applied, using only 70% of the samples per class to minimize distortions due to uneven sample distribution and to reduce potential classifier bias. The remaining 30% of the samples were reserved for subsequent accuracy assessment of the algorithm.

The statistical validation was performed using quantitative metrics derived from the confusion matrix, from which the following were calculated: Overall Accuracy (OA) (Equation (1)), which represents the proportion of correctly classified samples relative to the total number of samples; and Kappa Index (κ) (Equation (2)), which measures the agreement between classified and reference data while accounting for chance agreement.

$$OA = \frac{\left(\Sigma_{i=1}^{k} x_{ii}\right)}{N} \quad (1)$$

$$\kappa = \frac{\frac{\Sigma_{i=1}^{k} x_{ii}}{N} - \frac{\Sigma_{i=1}^{k}(x_{i+} * x_{+i})}{N^2}}{1 - \frac{\Sigma_{i=1}^{k}(x_{i+} * x_{+i})}{N^2}} \quad (2)$$

where x_{ii} is the number of correctly classified observations in class i (diagonal of the confusion matrix), x_{i+} and x_{+i} are the row and column totals, N is the total number

of observations, and k is the number of classes. Here, OA corresponds to the observed agreement, while κ accounts for the expected agreement by chance, ranging from −1 (worse than chance) to 1 (perfect agreement), with 0 indicating agreement equal to chance.

Figure 3. Examples of photographs taken during fieldwork: (**a**) Forest Formations, (**b**) Savanna Formations, (**c**) Grassland Formations, (**d**) Pasture, (**e**) Agricultural—Crops, and (**f**) Silviculture. Municipalities of Carolina, Riachão, Balsas, and Estreito, Maranhão State, Brazil (21–29 June 2021), and (11–19 February 2023). Source: the authors.

As it reflects the general level of classification precision, the overall accuracy is directly interpretable, since it corresponds to the general probability that a randomly selected region is correctly classified. The Kappa index is considered advantageous over overall accuracy, as it incorporates all elements of the error matrix, including both correctly and incorrectly classified objects [51]. Furthermore, it evaluates thematic accuracy more effectively due to its higher sensitivity to variations in commission and omission errors. The Kappa index ranges from −1 to 1, and the closer it is to 1, the higher the classification accuracy, being calculated based on the product of overall accuracy and commission errors [52].

For the construction of the confusion matrix and the calculation of the derived indices, a semi-structured selection of points was carried out, which varied according to the base year of the imagery, in addition to a set of 453 points collected during field visits conducted between 2019 and 2023 in the study area. For the year 2015, a total of 1605 points were used, comprising 231 forest formations, 258 savanna formations, 257 grassland formations, 281 pastures, 328 temporary crops, 154 silviculture, 52 exposed soil, and 44 water. The

validation of the 2020 classification was conducted using a total of 1819 samples, of which 301 were forest formations, 327 savanna formations, 274 grassland formations, 325 pastures, 350 temporary crops, 132 silviculture, 52 exposed soil, and 58 water. The results were compared to the performance thresholds established [53], who assigned qualitative characteristics to classification performance levels, thereby indicating the quality of the thematic map, as follows: (i) poor (Kappa < 0.0); (ii) slight (between 0.0 and 0.2); (iii) fair (between 0.2 and 0.4); (iv) moderate (between 0.4 and 0.6); (v) substantial (between 0.6 and 0.8); and (vi) almost perfect (Kappa > 0.8).

2.2.3. Dynamic Modeling

After the classification stage, scenario-building steps were carried out to project agricultural expansion trends in the Southern Maranhão mesoregion through the year 2030. Information on land cover changes between the 2015 (initial year) and 2020 (final year) maps was used, along with a set of variables that act as external factors to spatial changes, influencing the probability of a given transition occurring or not.

The appropriate selection of explanatory variables is a determining factor for the successful use of models. It is through their relationships with the dependent variable that the cells with higher or lower probability of land cover transition are defined, and these variables are organized into categorical and continuous types. Categorical variables correspond to information characterized by discrete classes—such as soil types and geology. Continuous variables, on the other hand, are measurable on a continuous scale, such as distance to primary and secondary roads, distance to rivers, distances to cities, distances to silos and warehouses, percentage of vegetation cover in the pixel, precipitation index, hypsometry, slope, and distance to conservation units.

The first step in the spatial modeling process in "Dinâmica EGO" is the definition of the transition rates that occur between classes, that is, the number of pixels from one class that change to another class within the analyzed period [6,7,38,39]. This process is carried out through the creation of the ergodic matrix, which enables the identification of the percentage of changes between classes based on global transition matrices. From these, bidimensional (simple) matrices are developed and subsequently discretized into annual matrices (multiple step), as shown in Equation (3) [13,42].

$$P^{\frac{1}{t}} = HV^{\frac{1}{t}}H^{-1} \quad (3)$$

P is the annual matrix, H and V are its eigenvectors and eigenvalues, and t corresponds to the analyzed period.

In "Dinâmica EGO", the transition matrix represents the probability of a cell changing its initial state, based on previously observed transitions, through the direct comparison between two maps (one representing the initial state and the other the final state). From this comparison, pixel change rates are calculated (e.g., the number of forest pixels in 2015 that were converted to agriculture in 2020) relative to the total number of pixels in the initial class (e.g., number of forest pixels in 2015). Subsequently, the probabilities of a pixel changing or not changing its state are calculated. Transition rate calculations were conducted for the nine transitions identified in the area and they represent the percentage of pixels that underwent class transitions in both the biennial analysis and the probabilistic period [6,10,12,52].

This choice reflects two dates (2015 and 2020) with a 5-year interval, effectively capturing the trend of natural Cerrado vegetation loss, as adopted by other studies in the region of Cerrado [10,11,15]. The longer time series tend to degrade the simulation data and introduce spurious trends. Using longer intervals can result in models with inconsistent

errors, as land use and land cover patterns—particularly those influenced by socioeconomic factors—are highly dynamic, and any structural change can generate inconsistent patterns.

2.2.4. Model Calibration

After the calculation of transitions, model calibration is performed in two stages. In the first stage, weights of evidence values are calculated for each of the identified transitions. In the second stage, a correlation analysis among the statistical variables is conducted. Since the weights of evidence method is based on the conditional probability of occurrence or non-occurrence of a transition, it requires the independence of each variable used. Therefore, it is necessary to remove those variables that show high correlation [54].

Based on Bayes' theorem of conditional probability, the weights of evidence method calculate the probability of transition of a cell based on its neighborhood—that is, it indicates the probability of occurrence of a transition $i \rightarrow j$ (e.g., forest to agriculture) due to the evidence provided by a statistical variable (e.g., roads), calculated according to Equations (4)–(7).

$$W^{+} = \ln\left(\frac{P(B|D)}{P(B|\overline{D})}\right) \tag{4}$$

$$W^{-} = \ln\left(\frac{P(\overline{B}|D)}{P(\overline{B}|\overline{D})}\right) \tag{5}$$

$$O(D|B) = O(D) * e^{W^{+}} \tag{6}$$

$$\log(O(D|B)) = \log(O(D)) + W^{+} \tag{7}$$

where $O(D)$ and $O(D \mid B)$ correspond, respectively, to the prior odds of the occurrence of event D and to the odds of D occurring given the presence of a pattern B (explanatory variable). W^{+} represents the positive weight of evidence, indicating a predisposition for the cell state to change, while W^{-} is the negative weight of evidence, reflecting resistance to the occurrence of event D, that is, a repulsion from the transition. Furthermore, non-significant values (close to zero) indicate that, within a given analysis range, the variable in question has no measurable effect on the transition [52].

Given a spatial pattern B, this is the posterior probability of a transition $i \rightarrow j$, using k spatial variables—that is, more than one spatial pattern is expressed by Equation (8) [7,9,13,55].

$$P\left(i \Rightarrow \frac{j(xy)}{V}\right) = \frac{\exp^{\Sigma_k w k n_{i \Rightarrow j(v)xy}}}{1 + \sum \exp^{\Sigma_k w k n_{i \Rightarrow j(v)xy}}} \tag{8}$$

where V refers to a vector of K spatial variables measured at location (x, y), each represented by its corresponding weight $W_{kn}^{i \rightarrow j}$, where $k = 1, \ldots, K$ is the index of the spatial variable, and $n = 1, \ldots, N_k$ is the index of the category of variable k (for categorical variables). $V_{kn}(x, y)$ indicates the value or indicator of category n of variable k at location (x, y). For continuous variables, the sum over n disappears, and it is sufficient to use $V_k(x, y)$. $W_{kn}^{i \rightarrow j}$ is the weight of variable k, category n (if applicable) for the transition $i \rightarrow j$. x, y are the spatial coordinates. In other words, the vector $V(x, y)$ contains the values of all spatial variables measured at the cell location in geographic space [56].

According to [10,52], for the application of the Weights of Evidence method, the variables must be discretized into class intervals, since the weight calculation is based on the occurrence or non-occurrence of a transition within the analyzed interval. The contrast is obtained from the difference between the positive and negative weights, as shown in Equation (9). The confidence level is derived from the contrast variance S^2 (C), presented in Equation (10), and indicates whether the analysis is statistically significant

at the 95% confidence level when $|C| > 1.96\ S(C)$, which confirms that the variable has a significant influence on the transition process [52,55,56].

$$C = W^{+} - W^{-} \tag{9}$$

$$S^2(C) = \frac{1}{P(B \cap D)} + \frac{1}{P(B \cap \overline{D})} + \frac{1}{P(\overline{B} \cap D)} + \frac{1}{P(\overline{B} \cap \overline{D})} \tag{10}$$

where (C) corresponds to the contrast, a statistic of interest that measures the difference between the positive and negative weights of evidence. (W^{+}) represents the positive weight, derived from the logarithm of the conditional probability of the event given the presence of a spatial variable, whereas (W^{-}) represents the negative weight, derived from the logarithm of the conditional probability of the event given the absence of that variable. $S^2(C)$ denotes the variance of the contrast, while S(C) is its standard deviation (the square root of the variance). B denotes event (or condition) 1, for example, the presence of a spatial variable or attribute, and D denotes event (or condition) 2, such as the occurrence of the target event (e.g., pasture expansion). $\overline{B}$ and $\overline{D}$ represent the complements of B and D, respectively, indicating their absence. P ($B \cap D$): probability that both B and D occur together; P ($B \cap \overline{D}$): probability that B occurs and D does not; P ($\overline{B} \cap D$): probability that B does not occur and D does; P ($\overline{B} \cap \overline{D}$): probability that neither B nor D occurs [57,58].

Contrast is used to measure both association and repulsion effects. Positive values favor the occurrence of a given transition within a specific range of the analyzed statistical variable [52,53]. Conversely, negative values indicate a repulsion to the same transition, and values close to zero can be disregarded (non-significant), as they do not influence the dynamic modeling process for that category [56]. This approach makes it possible to quantify influence, allowing inferences about how each variable may affect the conversion process in the area [52,53].

In the second stage, a correlation analysis among the statistical variables is carried out, since the weights of evidence method is based on the conditional probability of the occurrence or non-occurrence of a transition, requiring the independence of each variable used. Therefore, it is necessary to remove variables that exhibit high correlation. In "Dinâmica EGO", the Cramér's V and Joint Information Uncertainty (U) indices are used. Typically, U and V values greater than 0.50 indicate high correlation (strong dependence), and the static variable containing the highest number of non-significant values should be excluded. However, the criteria described in [52] were followed, and values greater than 0.40 for U and V were considered to indicate high correlation (Table 1), thus requiring their removal from the model. After the correlation analysis and the exclusion of dependent variables, the weights of evidence coefficients are recalculated, and their results are then incorporated into the simulation stages.

Table 1. Variables with values greater than 0.40 for study in the Southern Maranhão Mesoregion, Brazil.

Transition		Pair of Compared Variables		V	U
FF	PAS	Distance to UC	Precipitation *	0.45	0.31
FF	PAS	Geology *	Soils	0.44	0.18
FF	AGR	Distance to UC	Precipitation *	0.45	0.32
FF	AGR	Geology *	Soils	0.44	0.18
FF	SIL	Distance to UC *	Precipitation *	0.45	0.30
FF	SIL	Geology *	Soils	0.44	0.18
FS	PAS	Distance to UC	Precipitation *	0.46	0.33
FS	PAS	Geology *	Soils	0.44	0.18
FS	AGR	Distance to UC	Precipitation	0.47	0.33

Table 1. *Cont.*

Transition		Pair of Compared Variables		V	U
FS	AGR	Distance to silos	Distance to Silviculture *	0.43	0.10
FS	AGR	Geology *	Soils	0.44	0.18
FS	SIL	Distance to UC	Precipitation *	0.47	0.33
FS	SIL	Geology *	Soils	0.44	0.18
FC	PAS	Distance to UC	Precipitation *	0.47	0.33
FC	PAS	Distance to silos	Distance to Silviculture *	0.44	0.12
FC	PAS	Geology *	Soils	0.44	0.18
FC	AGR	Distance to UC	Precipitation *	0.46	0.33
FC	AGR	Distance to silos *	Distance to Silviculture	0.50	0.12
FC	AGR	Geology *	Soils	0.44	0.18
FC	SIL	Distance to UC	Precipitation *	0.47	0.33
FC	SIL	Distance to silos *	Distance to Silviculture	0.44	0.12
FC	SIL	Geology *	Soils	0.44	0.18

* Variables removed from the model for each analyzed transition. FF = Forest Formations; FS = Savanna Formations; FC = Grassland Formations; PAS = Pasture; AGR = Agriculture; SIL = Silviculture; UC = Conservation Units. Source: the authors.

2.2.5. Application of the Simulation Model

After the model calibration stage, the simulation is performed. For this, it is necessary to define the transition probability rates. In "Dinâmica EGO", this process is carried out using two functions: expander and patcher. The expander function is dedicated solely to the expansion or contraction of patches of a given class, while the patcher function is responsible for forming new patches. Both functions contribute to the creation of the transition probability map and are parameterized according to four properties: the pixel allocation rate, which defines the percentage of transition between classes; the isometry, which is a value ranging from 1 to 2 and determines the regularity of distances between the created patches; the variance; and finally, the average patch size, referring to the transitions analyzed between the initial and final maps [55]. Table 2 presents the expansion and patch parameters, defining the average sizes, variance, and isometry of the patches to be formed or expanded/contracted for the generation of the simulated landscape.

Table 2. Parameters used to generate the simulated landscape for the 2015–2020 simulation in the Southern Maranhão Mesoregion, Brazil.

	%			Average Size			Variance			Isometry		
	PAS	**AGR**	**SIL**	**PAS**	**AGR**	**SIL**	**PAS**	**AGR**	**SIL**	**PAS**	**AGR**	**SIL**
FF	0.90	0.80	0.80	3.24	4.05	1.72	22.34	46.99	13.85	1.50	1.50	1.50
FS	0.90	0.95	0.80	2.47	23.06	4.50	72.35	31,081.58	982.79	1.50	1.80	1.50
FC	0.90	0.85	0.80	6.13	11.29	4.41	230.44	1846.40	164.29	1.50	1.70	1.50

FF = Forest Formations; FS = Savanna Formations; FC = Grassland Formations; PAS = Pasture; AGR = Agriculture; SIL = Silviculture. Source: the authors.

The mean size and variance of patches were calculated using the average and standard deviation of converted areas, considering a minimum unit of one hectare (≈12 pixels) according to the segmentation standard. Transition analysis showed that 90% of converted cells expanded from preexisting areas, without generating new fragments, indicating a trend of conversion near consolidated agricultural zones. For pastures, 70–80% of conversions occurred over forest, savanna, or grassland formations. In the case of forestry, 80–90% of cells also showed expansion rather than fragmentation. These values were not

empirically defined but derived from the analysis of actual conversions, which shape the dynamics of class transitions. However, the spatial configuration of simulated areas, that is, the geometric pattern of converted patches, cannot be controlled.

As for isometry, a value of 1.5 was adopted for both the patcher and expander functions, resulting in more isometric (compact) rather than linear fragments. Isometry is a parameter that regulates the influence of spatial distance on transition probabilities and is associated with the fractal or geometric dimension of the neighborhood space. Its value ranges from 1 to 2. In "Dinâmica EGO", isometry defines how the spatial neighborhood influences land use dynamics, controlling the intensity of spatial effects on the transition process. The default value is 1.5, which enables calibration for different spatial patterns, such as more diffuse or more clustered transitions. In this study, the model was set to the default value of 1.5, as predefined by the "Dinâmica EGO" developers in the open-source configuration. The size of the new fragments was calculated based on the mapped area. Thus, their average size and variance were defined as 1 and 10 hectares, respectively, equivalent to 12 and 120 cells. These values were established by verifying the average sizes of transition areas. As a result, nine transition probability maps were generated for cells transitioning to pasture, agriculture, and silviculture, in which areas with a higher tendency toward spatial change can be identified [10,53,54].

2.2.6. Model Validation

In "Dinâmica EGO", model validation is performed using a multi-window analysis approach aimed at identifying the behavior of the data according to a neighborhood pattern. According to [6,9,10,13,33,56] the validation process in "Dinâmica EGO" is based on the concept of fuzziness of location. The model validation process aims to verify whether the model accurately represents the changes observed between the initial and final years. "Dinâmica EGO" uses a fuzzy similarity method for this purpose, calculated from the differences between the initial and simulated maps and between the initial and observed maps. This method is applied not pixel by pixel, but through multiple window sizes: 1×1, 3×3, 5×5, 7×7, and 11×11 [57,58].

Values are determined based on the distance from the central cell to the cell containing the class of interest within each comparison window, following a constant decay function. According to the literature, models with a minimum similarity of 0.40 or higher in windows of 7×7 or larger are considered acceptable [10,13,38,53]. Considering the spatial resolution of the data (30 m) and the resulting fit, simulations achieving a minimum validation score of 0.40 in 5×5 and 7×7 windows—corresponding to areas between 2.25 and 4.41 hectares—can be considered satisfactory, provided they visually approximate the mapped reality.

3. Results

3.1. Land Use and Land Cover—2015 and 2020

The classification standard proved to be relatively satisfactory, with the resulting maps presenting overall accuracy values of 71.53% for 2015 and 79.71% for 2020. The kappa coefficients were 0.663 for 2015 and 0.785 for 2020, classifying them as very good. Visually, the classifications also showed no significant inconsistencies, presenting a standard spatial pattern of class distribution in accordance with expectations.

Table 3 presents the results of land use and land cover (LULC) classes for 2015 and 2020 (in hectares), along with the respective differences calculated relative to 2020, both in absolute (hectares) and relative (%) terms. Positive values indicate an increase in area, while negative values indicate a reduction. It is noted that savanna (FS) and grassland (FC) formations together accounted for approximately 69% of the total area in 2015, highlighting their dominance over other land cover classes. During the period analyzed, these formations

experienced a combined loss of about 441,352 ha (−9.4%), indicating a significant reduction in native vegetation. In contrast, pasture and agricultural areas showed substantial growth, with increases of approximately 88,372 ha (16.2%) and 118,989 ha (14.5%), respectively, reflecting the conversion of natural landscapes into productive land uses.

Table 3. Land use and land cover for the Southern Maranhão Mesoregion, Brazil (2015–2020).

Classes LULC	Analyzed Period		Difference	
	2015	2020	(ha)	%
FF	646,687.98	880,015.80	233,327.80	36.08%
FS	2,343,552.84	2,016,165.00	−327,388.00	−13.97%
FC	2,332,351.26	2,218,387.00	−113,965.00	−4.89%
PAS	545,583.96	633,955.70	88,371.72	16.20%
AGR	820,765.98	939,754.60	118,988.60	14.50%
SIL	26,513.37	30,233.52	3720.15	14.03%
SE	438.57	696.51	257.94	58.81%
CH	42,347.52	36,786.51	−5561.01	−13.13%
AC	5684.13	7308.81	1624.68	28.58%

FF = Forest Formations; FS = Savanna Formations; FC = Grassland Formations; PAS = Pasture; AGR = Agriculture; SIL = Silviculture. SE = Exposed Soil; CH = Water; AC = Built-up Area. Source: the authors.

As previously mentioned, "Dinâmica EGO" calculates two types of information: the single-step transition matrix and the multi-step transition matrix. While the former records the percentage of cells that changed from one state to another over the period in a bi-temporal analysis (2015–2020), the latter calculates annual transition rates based on a Markov chain model, indicating the a priori probability of a cell being modified over time. This information is essential for understanding the dynamics of the cell conversion process and its behavior over the years. When analyzing the changes between 2015 and 2020, forest formations stand out with a 36% increase. This class gained area primarily from savanna formations and, to a lesser extent, from grassland formations.

Regarding conversion rates (Table 4), the transition from grassland formations (FC) to pasture (PAS) was the most pronounced, with a transition rate of 5.82%, followed by the conversion of savanna formations (FS) to agriculture (AGR) at 3.90%, and savanna formations (FS) to pasture (PAS) at 3.81%. During the 2015–2020 period, grassland formations experienced the highest conversion pressure, primarily to pasture, indicating the strong influence of livestock expansion on native vegetation loss. Savanna formations also exhibited considerable conversion, mainly to agriculture and pasture, reflecting the combined impact of cropping and grazing expansion. Forest formations (FF) presented lower transition rates but still showed notable losses, particularly to pasture (2.70%) and agriculture (0.66%).

Overall, these transitions demonstrate a consistent pattern of native vegetation replacement by pasture as the dominant land-use change, followed by agricultural expansion. The conversion from forest to pasture accounted for over 17 thousand hectares, while savanna and grassland formations collectively lost approximately 88 thousand hectares to pasture, 4 thousand hectares to agriculture, and 390 hectares to silviculture. These findings highlight the persistent anthropogenic pressure on native ecosystems in the Southern Maranhão Mesoregion and emphasize the need for targeted land management and conservation strategies.

There is a low probability of pasture expansion in the northeastern and central-southern parts of the region (Figure 4), particularly in the municipalities of Carolina and Riachão. The probability of conversion to silviculture showed the greatest discrepancies between observed and estimated data, with low overall expansion tendencies in the area. The highest probabilities were concentrated in the northwestern and northern portions of

the mesoregion, especially in the municipalities of Estreito, Carolina, São Pedro dos Crentes, Benedito Leite, São Félix de Balsas, and Loreto. After running the simulation routines, the validation was carried out by comparing the simulated map (2020) with the actual 2020 land cover map. This validation was conducted only for stationary scenarios, using the fuzzy similarity index according to window sizes of 1 × 1, 3 × 3, 5 × 5, 7 × 7, 9 × 9, and 11 × 11, as discussed.

Table 4. Land Cover transition (%) during the period from 2015 to 2020 in Southern Maranhão Mesoregion, Brazil.

Land Cover Transition 2015→2020	Global	Multiple (5 Years)
FF → PAS	2.70%	0.0060032
FF → AGR	0.66%	0.0005566
FS → SIL	0.06%	0.0000895
FS → PAS	3.81%	0.0088222
FS → AGR	3.90%	0.0091612
FS → SIL	0.20%	0.0005122
FC → PAS	5.82%	0.0145696
FC → AGR	2.10%	0.0038462
FC → SIL	0.08%	0.0001280

FF = Forest Formations; FS = Savanna Formations; FC = Grassland Formations; PAS = Pasture; AGR = Agriculture; SIL = Silviculture. Source: the authors.

It should also be emphasized that the terrain morphology influenced the transition to agricultural crops and planted pasture, with emphasis on flat areas, with slopes of up to 5% and altitudes up to 350 m, primarily favored by the mechanized farming practices in the region. Other regional and national studies also indicate that areas with gentler relief are prioritized for the expansion of pasture and grain cultivation [59,60]. In contrast, areas with slopes greater than 8% showed a strong tendency toward the expansion of pastures and silviculture. In general, lower-altitude areas, up to 160 m, correspond to the main floodplains of river channels that characterize the local drainage system, and are not directly used for commercial activities, resulting in low transition rates in these zones.

3.2. Validation Land Use and Land Cover

The simulated map showed a minimum similarity index of 0.45 and a maximum of 0.50 for 7 × 7 windows, indicating that the spatial arrangement of the adjusted variables is satisfactory, particularly considering the 30 m cell size. The minimum and maximum values were similar across 5 × 5 and 9 × 9 windows. According to [39], there is no single "correct" resolution for determining accuracy; values above 0.40 in 5 × 5 windows are generally considered acceptable, provided the spatial distribution patterns of the phenomenon in the reference and simulated maps are similar. Also notes that models adjusted with minimum values of 0.40 in 5 × 5 windows show significant accuracy, validating their use [55,56]. Simulations with fuzzy similarity indices between 0.45 and 0.50 for 7 × 7 to 11 × 11 windows demonstrate acceptable adjustments [52,53].

Considering the 30 m data resolution and the resulting fit, simulations with a minimum validation score of 0.40 in 5 × 5 to 7 × 7 windows (25–49 pixels, or 2.25–4.41 hectares) can be considered satisfactory, provided they visually approximate the mapped reality. The simulation of sugarcane expansion using 15 m resampled data obtained maximum similarity values below 0.45 in 7 × 7 windows [38], and simulating Amazon deforestation in "Dinâmica EGO" showed a minimum similarity of 0.40 between observed and simulated maps in 10 × 10 windows using 1 km resolution data [4].

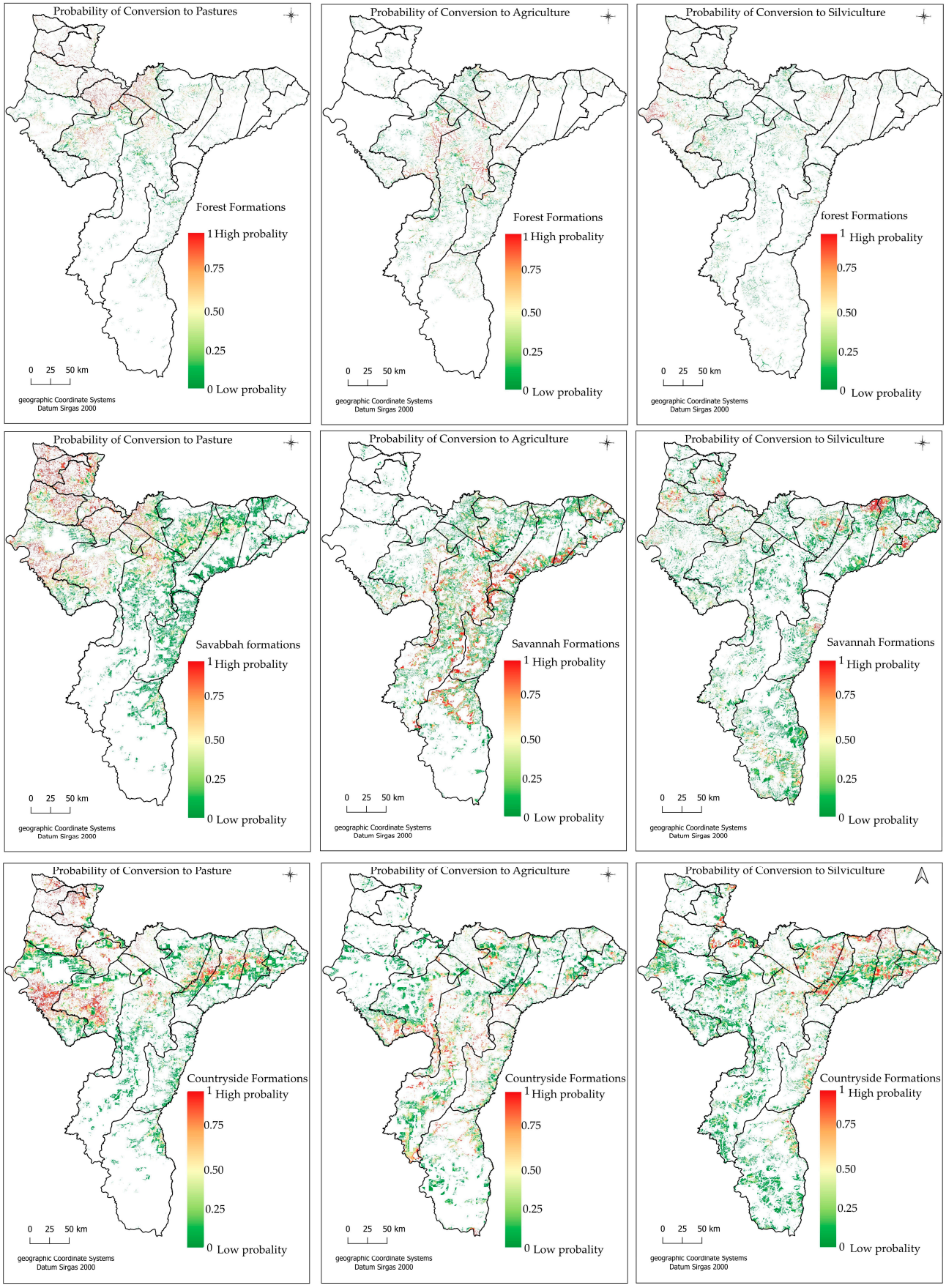

Figure 4. Spatial distribution of the probability of pasture expansion in the Southern Maranhão State Mesoregion, Brazil. Values range from 0 (low probability) to 1 (high probability). Source: the authors.

Figure 5 illustrates the comparison between the actual 2020 land use and land cover map and the simulated 2020 land use and land cover map, obtained through the calibration of the dynamic model for future scenarios.

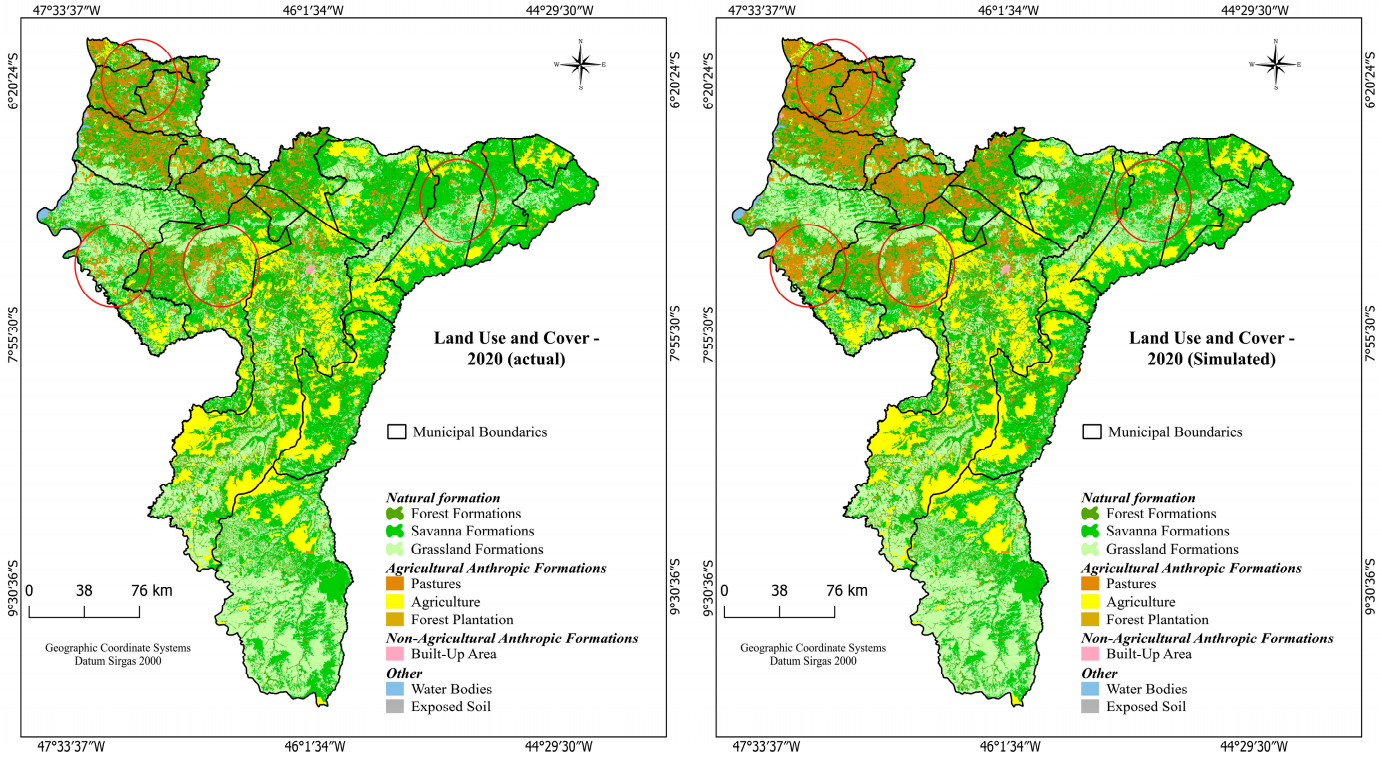

Figure 5. Comparison between the actual and simulated maps for the Southern Maranhão Mesoregion, Brazil. Red circles highlight the areas that showed the greatest differences when comparing actual and simulated data. Source: the authors.

The identified areas correspond to sectors that showed discrepancies between the actual and simulated data; however, a significant visual similarity between the two is evident—particularly in the agriculture and silviculture classes, which displayed good visual agreement. Nonetheless, the model overestimated the pasture class, especially in the northwestern portion of the study area, with emphasis on the municipalities of Campestre do Maranhão, Porto Franco, and São João do Paraíso. This class also showed area inconsistencies in the central portions of the municipalities of Carolina and Riachão.

It is also noted that the model failed to identify the emergence of new agricultural areas (patcher), and two main factors may explain this: first, during the calibration process, the model was not parameterized to analyze land-use modification processes (e.g., pasture→agriculture or agriculture→pasture); second, the model was calibrated to favor expansion (expander function) more heavily (95%) over the formation of new patches (patcher function at 5%) Despite this, the model was generally effective, as it achieved significant accuracy—for example, by correctly predicting no loss in protected natural vegetation remnants, such as those within the Chapada das Mesas National Park, and by not assigning land occupation to restricted areas. Table 5 compares the land areas between the actual and simulated datasets.

While in the actual 2020 data approximately 881 thousand hectares of forest formations were mapped, the 2020 simulated map computed 629 thousand hectares—representing a difference of 251 thousand hectares less compared to the actual data. Savanna formations showed a difference of 143 thousand hectares between the actual and simulated data: in 2020, this class totaled 2.0 million hectares (Mha) in the actual map, whereas the simulated

map identified approximately 2.2 Mha. Grassland formations presented a difference of around 70 thousand hectares between the actual and simulated datasets, with the simulated 2020 data showing the greatest tendency for loss in this class. In the actual 2020 data, grassland formations covered approximately 2.1 Mha, while in the simulated data, about 2.0 Mha were identified—much of which is associated with the expansion of pasture areas, as previously mentioned.

Table 5. Comparison between the mapped areas in the actual and simulated maps for the Southern Maranhão Mesoregion, Brazil in 2020.

Class/Year	2015	2020	2020 Simulate
FF	648,956.16	881,195.49	629,537.22
FS	2,417,991.48	2,073,583.89	2,216,923.3
FC	2,253,455.28	2,146,511.88	2,075,932.9
PAS	543,325.05	629,712.45	783,643.86
AGR	824,283.54	954,986.85	974,510.37
SIL	28,284.57	33,288.21	360,66.96
SE	407.25	680.67	407.25
CH	41,439.78	36,401.22	41,443.83
AC	5801.49	7583.94	5801.49

FF = Forest Formations; FS = Savanna Formations; FC = Grassland Formations; PAS = Pasture; AGR = Agriculture; SIL = Silviculture; SE = Exposed Soil; CH = Water; AC = Built-up Area. Source: the authors.

Pasture is among the land cover classes with the greatest differences in area between the actual and simulated data. In the actual 2020 map, approximately 629 thousand hectares of pasture were mapped, whereas the 2020 simulated map showed 783 thousand hectares—indicating an overestimation of this class in the simulated model.

Agriculture and silviculture, on the other hand, showed relative stability between the actual and simulated data when analyzing the spatial distribution of these classes in the study area. Agriculture presented a difference of just over 19 thousand hectares between the actual and simulated maps. In the actual 2020 map, agriculture occupied around 954 thousand hectares, while in the simulated map it covered approximately 974 thousand hectares. Silviculture showed a difference of nearly 2.7 thousand hectares, with the actual map recording an area close to 33 thousand hectares, and the simulated map indicating more than 36 thousand hectares of land covered by silviculture (Table 6).

Table 6. Cross-tabulation between actual and simulated data for the year 2020 in Southern Maranhão Mesoregion, Brazil.

		2020 Simulated								
		FF	**FS**	**FC**	**PAS**	**AGR**	**SIL**	**SE**	**CH**	**AC**
2020 Actual	FF	54.15%	33.38%	5.10%	* 4.86%	* 1.95%	* 0.13%	0.00%	0.43%	0.00%
	FS	5.26%	67.36%	16.63%	* 6.16%	* 4.07%	* 0.29%	0.00%	0.23%	0.00%
	FC	1.01%	17.20%	72.58%	* 6.96%	* 2.00%	* 0.12%	0.01%	0.11%	0.02%
	PAS	2.45%	11.14%	14.53%	70.25%	1.36%	0.16%	0.01%	0.07%	0.03%
	AGR	0.43%	8.36%	3.45%	1.77%	85.90%	0.07%	0.00%	0.01%	0.00%
	SIL	1.00%	12.24%	5.02%	5.44%	2.46%	73.81%	0.00%	0.02%	0.00%
	SE	0.63%	12.05%	24.78%	20.64%	0.37%	6.94%	22.70%	10.82%	1.07%
	CH	4.57%	6.20%	3.03%	2.94%	0.70%	0.08%	0.01%	82.44%	0.02%
	AC	0.60%	5.33%	8.66%	18.05%	0.21%	0.00%	0.00%	0.19%	66.97%

* Transition classes considered in the model. FF = Forest Formations; FS = Savanna Formations; FC = Grassland Formations; PAS = Pasture; AGR = Agriculture; SIL = Silviculture; SE = Exposed Soil; CH = Water; AC = Built-up Area. Source: the authors.

As observed, the comparison between the actual and simulated maps for the year 2020 showed a significant rate of class persistence. The greatest inconsistencies were found in forest formations, which had a permanence rate of 54%—the lowest among the analyzed land cover classes. The other classes showed compatibility rates above 60%, with the best results for pasture and agriculture, with permanence rates of 70% and 85%, respectively. A relative area gain was noted in the comparison between the actual and simulated maps, with error rates ranging from 4% to 7%, generally involving notable confusion between savanna formations and pasture, as well as between grassland formations and pasture. These showed confusion rates between 2% and 7% when comparing the actual and simulated maps for the year 2020.

3.3. Simulation of Land Use and Land Cover—2020/2030

The accuracy assessment indicated satisfactory classification performance, with an overall accuracy of 70.3% and a Kappa coefficient of 0.61, representing a good agreement between the land use and land cover map classified and the simulated land use and land. In terms of area, the simulated model showed that between 2020 and 2030, natural Cerrado vegetation is projected to lose over 842 thousand hectares, a figure close to that observed between 1990 and 2020, when approximately 1.2 million hectares (Mha) of native biome vegetation were converted into anthropic land use classes in the region. The greatest tendency for conversion is associated with the expansion of pasture, followed by agriculture, with a lower tendency for conversion into silviculture.

Figure 6 illustrates the spatial distribution of land use and land cover classes between the years 1990 and 2030-S. It is important to note that the information from 1990 to 2020 refers to actual land cover values obtained through digital image classification, whereas the data beyond 2020 correspond to land use and land cover scenarios generated by the static simulation model.

The model indicates that areas classified as grassland formations show a significant tendency for conversion, with an estimated reduction of approximately 310 thousand hectares between 2020 and 2030—that is, decreasing from an area of 2.21 million hectares (Mha) in 2020 to a projected area of 1.83 Mha in the 2030 simulated model. The main losses in this class are projected to pasture, with over 289 thousand hectares converted, followed by agriculture, with a projected conversion of approximately 72 thousand hectares. Silviculture showed a projected increase of 2.6 thousand hectares over grassland formations.

Although not explicitly incorporated into the model, grassland formations experienced a minor gain of 52 thousand hectares from savanna formations. Savanna formations showed the highest loss rates between the actual period and the simulated scenario for 2030, with a decrease of 437 thousand hectares—from 2.0 Mha in 2020 to 1.6 Mha in the 2030 simulated map. This class demonstrated a significant tendency for conversion to agriculture, with projections indicating a loss of around 190 thousand hectares. In the simulated scenario, a high tendency for pasture expansion over savanna formations was evident, with an estimated 185 thousand hectares of savannas converted into pasture. Additionally, just over 8.6 thousand hectares of savanna formations showed a projected conversion to silviculture.

Although less intense, forest formations showed a relative probability of area loss. Between 2020 and the 2030 simulated data, there is a projected loss of over 85 thousand hectares of forest formations in the area. Most of this conversion is linked to pasture expansion: according to the simulated model, approximately 75 thousand hectares of forest formations were converted into pasture, just over 8.7 thousand hectares were converted into agriculture, and 519 hectares into silviculture.

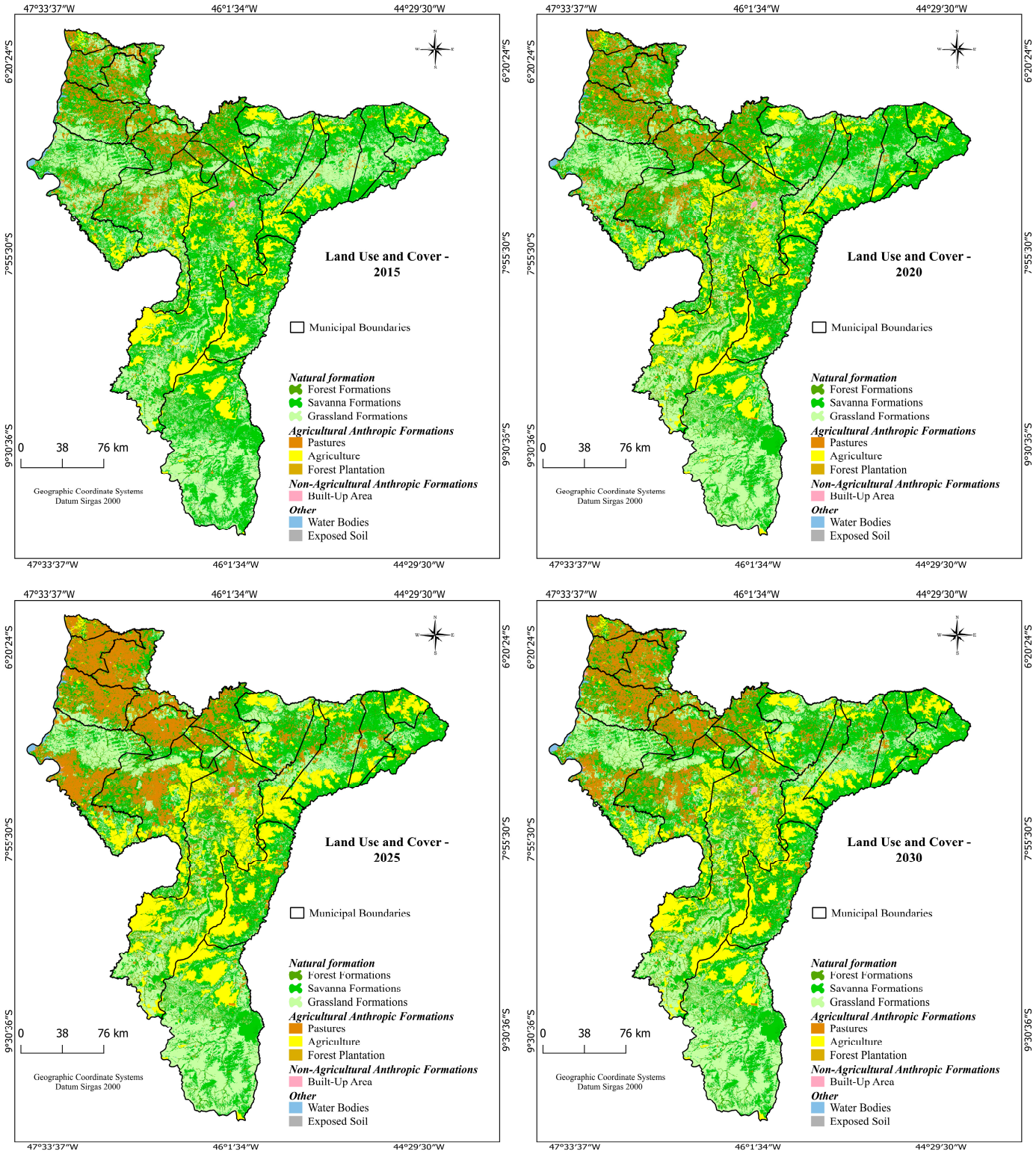

Figure 6. Land use and land cover in the Southern Maranhão Mesoregion, Brazil (2015–2030). Source: the authors.

4. Discussion

4.1. Dynamics of Land Use and Land Cover—2015 and 2020

The land use and land cover classification process was also refined, generally eliminating confusion between classes. The greatest inconsistencies occurred between pastures, agricultural areas, and grassland formations. This is due to the significant spatial proximity

of these classes, especially during the dry season [10–13]. The resulting data presented global accuracy and kappa with values greater than 85%, with the 2015 classification presenting values of 0.822 and 86% for kappa and global accuracy and the 2020 classification presenting values of 0.899 and 92% for kappa and global accuracy, respectively.

This result may be associated with the natural regeneration process of areas in the Cerrado, which has been observed by different authors in other recent studies of this biome [40,61,62]. Notably, the classification process was refined, generally eliminating confusion between classes. For the forest formation class, an accuracy of approximately 95% was observed in both analyzed years (1995 and 2000). Additionally, possible phenological issues related to the period/year of the analyzed images may also influence the results at a small scale.

The savanna formations showed a trend of loss, with a reduction of approximately 13%, converted mainly into agricultural land and, to a lesser degree, into pasture. A similar pattern was observed for grassland formations, which lost about 5% of their area. The most significant area gain was observed in pasturelands, which expanded by more than 16%, followed by the agriculture and silviculture classes, which increased their area by 14% over five years.

The weights of evidence analysis indicated that the variables "distance to pasture" (Table 4), "distance to agriculture," and "distance to silviculture" showed positive weights up to 3 km—meaning that areas near already consolidated land have a greater tendency for conversion to both pasture and agriculture, with this influence decreasing as the distance from these variables increases. Although positive, the variables "distance to roads," "distance to silos," and "precipitation" did not prove to be significant drivers for the conversion of natural areas into anthropogenic uses. Their influence was greater within the first 500 m but became negligible beyond that distance. Moreover, these variables had weights close to zero, indicating little influence on the conversion process in the area. On the other hand, the variables "distance to drainage" and "distance to protected areas" act as inhibitors to agricultural expansion; however, their values were also close to zero, suggesting that, even though legally protected, these areas do not constitute an entirely effective barrier against deforestation in the region.

Similar results were found by [38,54] when analyzing sugarcane expansion, observing positive weights of evidence at distances between 2 and 8 km from agricultural areas. In turn, when modeling deforestation scenarios for the Cerrado, identified the strong influence of already consolidated soybean cultivation regions as the main driver of deforestation expansion throughout the area, particularly within a 3 km range. According to [54], in the Cerrado biome, proximity to already consolidated areas—whether for urbanization or agricultural purposes—tends to attract new areas as occupation advances. Thus, based on the evaluation of weights of evidence values, it was necessary to define some adjustment parameters, such as transition rates, which determine the amount of area involved in each trend of change evaluated, and the quantity of land cover change. These were defined based on patcher and expander values, which determine location accuracy and the percentage of transitions assigned to the expansion of existing areas or the creation of new land cover patches. The patcher and expander values were defined according to average size, variance, and isometry [10,57].

The expansion of agriculture shows a stronger tendency to occur in the central-southern portion of the mesoregion, extending toward the northeast, particularly over flat topography generally covered by Latosols—one of the main characteristics of areas susceptible to agricultural conversion. Notable examples include the chapadas and chapadões that make up the Serra do Penitente. These areas exhibited a high probability of conversion to agriculture, especially in the municipalities of Balsas, Tasso Fragoso, Alto

Parnaíba, and São Raimundo das Mangabeiras, as well as the southern portion of Carolina and the northern portion of Riachão. Pasturelands showed a higher probability of conversion in the northwestern portion of the region, mainly over grassland formations, predominantly in the municipalities of Campestre do Maranhão, Porto Franco, São João do Paraíso, Feira Nova, Carolina, and Estreito, as well as the northern area of Balsas. These areas correspond to zones with lower potential for mechanized agriculture and a higher occurrence of Plinthosols.

4.2. Analysis of the Simulation of Land Use and Land Cover—2020/2030

The projection phase for agricultural and livestock expansion in the Southern Maranhão Mesoregion used the 2020 land use and land cover map as a starting point, applying the same calibration parameters (transition matrix, weights of evidence file, and statistical variables) from the validated 2015 model. The land use and land cover dynamics indicated that between 2020 and 2030, the model emphasized trends already observed between 2015 and 2020, particularly highlighting the expansion of pasture and, to a lesser extent, the increase in agriculture, with projected expansions of 88% and 29%, respectively. Silviculture, although showing relative growth with a projected expansion of approximately 45% by 2030, remained stable within the projected scenario.

In contrast, natural Cerrado vegetation showed significant projected losses, with rates around 19% in the simulation map for 2030. Notably, even though it was not directly considered in this stage of the analysis, the presence of special areas (strict and sustainable-use conservation units) demonstrated considerable effectiveness in controlling the loss of natural Cerrado vegetation. The simulated model indicated that the largest remnants of natural vegetation projected to remain by 2030 are located within protected areas—such as Chapada das Mesas National Park (Parna da Chapada das Mesas), Nascentes do Rio Parnaíba National Park (Parna Nascentes do Rio Parnaíba), and, to a lesser extent, the Nascentes do Rio Balsas Environmental Protection Area (APA Nascentes do Rio Balsas).

On the other hand, the area still contains a vast amount of land with natural Cerrado vegetation that is legally available for conversion, placing it at the center of discussions on environmental conservation, economic development, and natural resource management [29]. The presence of these unconverted areas can be a decisive factor for agricultural expansion, particularly because they retain a significant coverage of native vegetation. Unlike the Amazon, where legal protection reaches 80%, the Cerrado requires only 35% Legal Reserve according to the Forest Code (Law No. 12.651/2012), making it more vulnerable to conversion by increasing the availability of areas legally suitable for agriculture. Additionally, the emergence of production incentive public programs and policies promoting agribusiness put further pressure on these remaining regions, reinforcing the perception of the Cerrado as a strategic agricultural frontier. Thus, the combination of lower legal protection and the presence of unconverted land favors agricultural expansion, while simultaneously jeopardizing the conservation of the biome's biodiversity and ecosystem services.

This data reveals that (Table 6 and Figure 6), although already established as an agricultural frontier, the area shows a strong tendency for agricultural and livestock expansion. Between 2020 and 2030, the model projects a potential expansion of over 833 thousand hectares, of which 564 thousand hectares are destined for pasture, 258 thousand hectares for agriculture, and just over 10 thousand hectares for silviculture. As previously mentioned, the pasture class showed the greatest tendency to expand over grassland and savanna formations. However, even though it was not explicitly included in the predictive model, a small area of agriculture was observed to have been converted into pasture (≈13 thousand hectares), indicating the model's potential to project land use changes from one agricultural class to another.

Despite being a consolidated agricultural frontier, the Southern Maranhão Mesoregion continues to show a strong trend toward agro-pastoral expansion, mainly the replacement of natural vegetation by pasture and, to a lesser extent, by cropland and silviculture, reinforcing the ongoing pressure on native ecosystems. This pattern is not spatially uniform, as the municipalities comprising the microregions of Porto Franco and Gerais de Balsas show significant projected conversion of grassland and savanna formations into pasture and agriculture.

The conversion of forest formations is primarily concentrated in the northwestern portion of the area, within the transition zone between the Amazon and Cerrado biomes. This region showed a strong tendency for the loss of grassland formations to pasture, with notable changes in the municipalities of Porto Franco, Carolina, São João do Paraíso, Estreito, and Feira Nova do Maranhão. Meanwhile, the central portion of the mesorgion showed a high projected expansion of agriculture, especially in the municipalities of Balsas, Tasso Fragoso, São Raimundo das Mangabeiras, and the southern part of Sambaíba.

This scenario is consistent with the estimates of [10], who, when simulating deforestation processes in the Cerrado using resampled data from MapBiomas Collection 7 [63], indicated a high probability of conversion of native vegetation to pasture (≈4.7 million hectares) and to agriculture (≈1.4 million hectares), as well as a significant tendency for agricultural expansion over pasture (≈3.2 million hectares), which was not tested in the present model. The same author also highlights the municipality of Balsas-MA as one of the three municipalities with the highest estimated conversion of native vegetation and among the ten municipalities in the Cerrado with the greatest environmental risk associated with deforestation by 2030.

Modeling deforestation scenarios for the MATOPIBA region through 2050 projected a reduction of 21% to 24% in the Cerrado's natural vegetation, along with a marked trend of expansion in pasturelands and agricultural areas [38]. When developing a simulation model for the entire Cerrado biome, [57] showed that even under optimistic scenarios—such as those involving the implementation of conservation policies and restrictions on deforestation in special areas—there are still high estimates of vegetation cover loss in the Cerrado. It is noteworthy that the aforementioned authors identified the region bordering the Amazon biome—which includes the area under study—as showing a significant trend toward vegetation loss.

Finally, it is important to emphasize that the simulation of agricultural expansion does not precisely measure spatial variation across the area, as it is influenced by political, economic, and social factors. However, the model developed and presented here allows for the analysis of the trend of natural vegetation cover loss, since it identifies areas that are relatively vulnerable to the deforestation process. As the model was not calibrated to detect trends in vegetation regeneration or the expansion of agriculture over pasture, it revealed a strong tendency toward natural vegetation loss.

4.3. Geospatial Approaches, Policy Implications and Future Research Directions

Several studies have demonstrated that geomatic approaches play a central role in advancing the understanding of land use and land cover dynamics in different regions, by integrating spatial modeling, remote sensing, and geographic information systems (GIS). For example, [64] used multitemporal Landsat imagery and Random Forest classification to elucidate long-term land use and land cover changes in South Africa, contributing to more effective environmental management and sustainable land-use policies. Similarly, [65] combined Landsat data, GIS frameworks, and Random Forest algorithms to analyze the spatiotemporal dynamics of degradation in Burkina Faso, highlighting how geospatial

tools enable robust monitoring systems aligned with the sustainable management of protected areas.

Gong et al. [66] demonstrated the transferability of high-resolution land cover mapping by leveraging a limited 30 m sample set to generate a 10 m global land cover map, reinforcing the potential of machine learning and remote sensing integration for large-scale environmental monitoring. However, the effectiveness of the method applied in this study is directly related to the minimum mapping unit (MMU) and the spatial scale of the input data. For all image sets analyzed in the Southern Maranhão Mesoregion, a similarity threshold of 0.010 and a minimum area of 12 pixels, corresponding to approximately one hectare, was selected, considering the 30 m spatial resolution. These settings provided the most accurate representation of objects in the images, ensuring that the segmentation captured meaningful landscape features while minimizing over or under-segmentation. Smaller MMUs could allow detection of finer landscape features but would increase classification noise, whereas larger MMUs tend to generalize patterns and reduce detail. Therefore, the method's performance and comparability across scales depend on balancing spatial resolution, mapping objectives, and the degree of landscape fragmentation in the study area.

In Brazil, a study used the Landsat archive and the Google Earth Engine platform to reconstruct three decades of land use and land cover changes across all major biomes, including the Cerrado [67], providing valuable insights into long-term land use trajectories. Comparative analyses with other studies conducted in tropical savannas and agricultural frontiers around the world reveal that the land use dynamics observed in the Southern Maranhão Mesoregion follow global patterns of agricultural expansion and ecosystem conversion. Large-scale land use transformations are among the main drivers of global biogeochemical and hydrological changes, establishing direct links between local land management and global impacts [1]. It is also noteworthy that socioeconomic and institutional factors, such as market forces, infrastructure development, and shifts in public policies, are universal determinants of land use and land cover changes in tropical regions [2]. Similarly, the growing influence of industrial drivers of deforestation in tropical ecosystems is emphasized, a trend reflected in the mechanized agricultural expansion observed in the MATOPIBA region of Brazil [3].

At the regional scale, Rau et al. [68] modeled past and future forest cover scenarios in the Misiones Forest, Argentina, showing that agricultural intensification and land tenure patterns strongly influence deforestation trajectories, results consistent with those found in this study. Similar spatiotemporal patterns of conversion from native vegetation to agricultural land have also been reported in other savanna regions, especially under demographic pressure and in contexts of limited land governance [64,65]. In East Africa, a study applied a hybrid ANN–CA–Markov modeling framework in Ethiopia, successfully predicting land use transitions driven by both natural and anthropogenic factors [33]. These interregional studies demonstrate that the processes identified in the Brazilian Cerrado are part of broader global transformations affecting tropical savannas, reinforcing the global relevance of this research and highlighting the importance of predictive geomatic modeling to support more sustainable land management.

In this context, recent debates on amendments to the Brazilian Forest Code have emphasized the relaxation of environmental protection regulations, which may lead to increased deforestation, especially affecting remnant grassland vegetation. For example, Bill no. 364/2019 [69], if approved, would allow the use of over 50% of the Pantanal, 32% of the Pampas, and 7% of the Cerrado. This political context makes the modeling presented in this study even more relevant, as approximately 2.0 million hectares of grassland formations with significant conversion probability to agricultural use were identified in the Southern Maranhão Mesoregion, areas crucial for aquifer recharge and biodiversity maintenance.

On the other hand, emerging policies such as the National Program for the Conversion of Degraded Pastures into Sustainable Agricultural and Forestry Production Systems (PNCPD) [70] offer concrete pathways to reduce pressure on natural areas by promoting productive and ecological recovery of degraded pastures. Considering that the Southern Maranhão Mesoregion has just over 1% of its pastures in degraded condition [63], incentivizing the adoption of this program could be an effective strategy to reduce deforestation associated with agricultural expansion.

Based on the results of this research, it is recommended that public policies aimed at territorial management in the Cerrado and other tropical savannas prioritize: (i) the use of predictive spatial modeling, such as that developed here, to support ecological-economic zoning and guide the allocation of new productive activities, ensuring the preservation of native vegetation remnants; (ii) strengthening regulatory and economic instruments that encourage the recovery of degraded areas through sustainable production systems, avoiding the replacement of native areas; (iii) integrating geospatial and socioeconomic information into management plans and sectorial policies for more effective and territorially targeted decisions; (iv) critically reviewing and restricting legislative proposals that relax environmental norms, preventing setbacks that compromise biome conservation, especially in environmentally sensitive areas identified by the model; and (v) promoting community participation and strengthening local governance for environmental monitoring and enforcement.

The modeling framework developed in this study could be extended to other savanna regions in Brazil and other countries. Naturally, it would be necessary to adapt the input datasets and recalibrate the model parameters to local conditions. Future research should simulate land use and land cover changes under diverse socioeconomic and policy scenarios to support strategic planning and environmental conservation. Expanding this approach will enable the identification of vulnerable areas, deforestation hotspots, and priority zones for sustainable management, thereby broadening the application of geospatial modeling in agro-environmental monitoring. Furthermore, future studies should examine the pressures of agricultural expansion on protected areas and adjacent landscapes, addressing social, economic, and environmental factors such as deforestation, land speculation, infrastructure development, logistics, and public asset management.

Additionally, refining and testing alternative land use scenarios within various socioeconomic and institutional frameworks, integrating the model proposed here, will be critical. These efforts should assess the impacts of conservation policies, economic incentives, and regulatory changes, especially in regions facing intense agricultural expansion. This research will enhance the identification of vulnerable regions, improve public policy assessments, and guide sustainable land management practices, strengthening the integration between geospatial modeling and decision-making processes to balance production and conservation in tropical biomes.

5. Conclusions

The results of this study underscore the critical role of advanced geospatial technologies and machine learning in providing accurate and reliable insights into land use and land cover dynamics in the Cerrado biome in Brazil. By integrating remote sensing data, spatial analysis, and predictive modeling, this research generated georeferenced information that supports informed decision-making (public and private), effective agro-environmental monitoring, and sustainable resource management. The thematic maps produced, using the Random Forest algorithm, revealed clear spatial patterns of vegetation loss and agricultural expansion, offering valuable guidance for identifying vulnerable areas and prioritizing conservation and land management efforts.

The analysis of land use and land cover dynamics in the study area revealed that, although the natural Cerrado vegetation (forests, grasslands, and savanna formations) still covers more than 75% of the area, significant losses were observed during the analyzed period, primarily in savannas converted into agricultural areas and, to a lesser extent, pastures. Grasslands showed relative stability, while agricultural expansion led among the anthropogenic classes, followed by pastures and silviculture.

Projections up to 2030, considering pessimistic scenarios without natural regeneration, indicate that the proximity to already converted areas increases the likelihood of further conversions, highlighting that factors such as proximity to roads have a lesser influence in this region due to the consolidation of agriculture near major roads. The model suggests a continued trend of natural vegetation conversion, with projected loss rates between 10% and 13%, similar to those observed over the past three decades, with pasture expansion exerting the greatest pressure on the Cerrado in southern Maranhão state, followed by agricultural areas, and lesser pressure from silviculture.

Given the discussion presented, future studies should be expanded through new analyses that incorporate alternative classification methods, class separability criteria, and parameter adjustments, considering the high diversity of land use in the Cerrado biome. Additionally, future research should include the analysis of regeneration processes and optimistic scenario modeling, adopting land cover patterns with lower conversion rates or incorporating calibration based on conservation units, aiming to mitigate the impacts of agricultural expansion and conserve biodiversity in rapidly changing landscapes.

Author Contributions: Conceptualization, P.R.M.P. and É.L.B.; methodology, P.R.M.P. and É.L.B.; formal analysis, P.R.M.P., É.L.B., F.W.D.C., T.C.S.R., M.S.F.F. and E.V.B.; investigation, P.R.M.P.; resources, P.R.M.P. and É.L.B.; data curation, P.R.M.P., É.L.B., F.W.D.C., T.C.S.R., M.S.F.F. and E.V.B.; writing—original draft preparation, P.R.M.P.; writing—review and editing, P.R.M.P., É.L.B., F.W.D.C., T.C.S.R., M.S.F.F. and E.V.B.; visualization, P.R.M.P., É.L.B., F.W.D.C., T.C.S.R., M.S.F.F. and E.V.B.; supervision, É.L.B.; project administration, P.R.M.P. and É.L.B.; funding acquisition, P.R.M.P. and É.L.B. All authors have read and agreed to the published version of the manuscript.

Funding: This research was funded by CAPES—Coordination for the Improvement of Higher Education Personnel/Doctoral Scholarship (P.R.M.P.), National Council for Scientific and Technological Development (CNPq)/Research Productivity Fellowship (Grant #302963/2025-1) (E.L.B) and FAPESP—São Paulo Research Foundation (Grant #2019/26222-6 and #2022/09319-9) (E.L.B.).

Data Availability Statement: The data presented in this study are available upon request to the corresponding author.

Conflicts of Interest: Author E.L.B. was employed by the public company Brazilian Agricultural Research Corporation. The remaining authors declare that the research was conducted in the absence of any commercial or financial relationships that could be construed as a potential conflict of interest.

Abbreviations

The following abbreviations are used throughout this manuscript for clarity and consistency:

AC	Built-up Area
AGR	Agriculture
CH	Water
CSR	Remote Sensing Center, Federal University of Minas Gerais
Dinâmica EGO	Environment for Geoprocessing Objects (software version 8.3.0)
DIS	Distance
EVI	Enhanced Vegetation Index
FC	Grassland Formations
FF	Forest Formations

FS	Savanna Formations
GDP	Gross Domestic Product
GIS	Geographic Information Systems
LULC	Land Use and Land Cover
MATOPIBA	Region formed by the states of Maranhão, Tocantins, Piauí, and Bahia
Mha	Million Hectares
MMU	Minimum Mapping Unit
NDVI	Normalized Difference Vegetation Index
NDBI	Normalized Difference Built-up Index
NDWI	Normalized Difference Water Index
PAS	Pasture
PCA	Principal Component Analysis
PRODECER	Japanese-Brazilian Cooperation Program for the Development of the Cerrado
RF	Random Forest
SAVI	Soil-Adjusted Vegetation Index
SE	Exposed Soil
SIL	Silviculture
UFMG	Federal University of Minas Gerais
USGS	United States Geological Survey

References

1. Foley, J.A.; Defries, R.; Asner, G.P.; Barford, C.; Bonan, G.; Carpenter, S.R.; Chapin, F.S.; Coe, M.T.; Daily, G.C.; Gibbs, H.K. Global consequences of land use. *Science* **2005**, *309*, 570–574. [CrossRef]
2. Lambin, E.F.; Turner, B.L.; Geist, H.J.; Agbola, S.B.; Angelsen, A.; Bruce, J.W.; Coomes, O.T.; Dirzo, R.; Fisher, G.; Folke, C.; et al. The Causes of Land-Use and Land-Cover Change: Moving Beyond the Myths. *Glob. Environ. Change* **2001**, *11*, 261–269. [CrossRef]
3. Austin, K.G.; González-Roglich, M.; Schaffer-Smith, D.; Schwantes, A.M.; Swenson, J.J. Trends in size of tropical deforestation events signal increasing dominance of industrial-scale drivers. *Environ. Res. Lett.* **2017**, *12*, 054009. [CrossRef]
4. Maeda, E.E.; Almeida, C.M.d.; Ximenes, A.d.C.; Formaggio, A.R.; Shimabukuro, Y.E.; Pellikka, P. Dynamic modeling of forest conversion: Simulation of past and future scenarios of rural activities expansion in the fringes of the Xingu National Park, Brazilian Amazon. *Int. J. Appl. Earth Obs. Geoinf.* **2011**, *13*, 435–446. [CrossRef]
5. Burrough, P.A. *Principles of Geographical Information Systems for Land Resources Assessment*; Clarendon Press: Oxford, UK, 1994; 193p.
6. Soares-Filho, B.S. Modelagem da Dinâmica de Paisagem de Uma Região de Fronteira de Colonização Amazônica. Ph.D. Thesis, Escola Politécnica, Universidade de São Paulo, São Paulo, Brazil, 1998.
7. Pedrosa, B.M.; Camara, G. Modelagem dinâmica e sistemas de informações geográficas. In *Geomática: Modelos e Aplicações Ambientais*; Meirelles, M.S.P., Camara, G., Almeida, C., Eds.; Embrapa Informação Tecnológica: Brasília, Brazil, 2007.
8. Benedetti, A.C.P. Modelagem Dinâmica para a Simulação de Mudanças na Cobertura Florestal das Serras do Sudeste e Campanha Meridional do Rio Grande do Sul. Ph.D. Thesis, Centro de Ciências Rurais, Universidade Federal de Santa Maria, Santa Maria, Brazil, 2010.
9. Pavão, M. Modelagem e Análise de Mudanças do uso e Cobertura da Terra no Entorno de áreas Protegidas: O caso do Parque Estadual da Cantareira, São Paulo. Ph.D. Thesis, Faculdade de Filosofia, Letras e Ciências Humanas, Universidade de São Paulo, São Paulo, Brazil, 2017.
10. Nogueira, S.H.M. Desmatamentos no Bioma Cerrado: Contextos, Padrões e Tendências, Impactos e Alternativas. Ph.D. Thesis, Curso de Ciências Ambientais, Universidade Federal de Goiás, Goiânia, Brazil, 2022.
11. Molin, P.G. Dynamic Modeling of Native Vegetation in the Piracicaba River Basin and Its Effects on Ecosystem Services. Ph.D. Thesis, Escola Superior de Agricultura "Luiz de Queiroz", Universidade de São Paulo, Piracicaba, Brazil, 2014.
12. Pereira, P.R.M.; Costa, F.W.D.; Bolfe, É.L.; Macarringe, L.; Botelho, A.C. Comparison of classification algorithms of images for the mapping of the land covering in Tasso Fragoso municipality, Brazil. *ISPRS Ann. Photogramm. Remote Sens. Spat. Inf. Sci.* **2021**, *3*, 167–173. [CrossRef]
13. Pereira, P.R.M. Modelagem Dinâmica de Uso e Cobertura da Terra Para Mesorregião sul Maranhense. Ph.D. Thesis, Instituto de Geociências, Universidade Estadual de Campinas, Campinas, Brazil, 2024.
14. Inicêncio, M.E. O Proceder e as Tramas do Poder na Territorialização do Capital no Cerrado. Ph.D. Thesis, Instituto de Estudos Sócio-Ambientais, Universidade Federal de Goiás, Goiânia, Brazil, 2010.

15. Polizel, S.P.; Vieira, R.M.S.P.; Pompeu, J.; Ferreira, Y.C.; Sousa-Neto, E.R.; Barbosa, A.A.; Ometto, J.P.H.B. Analysing the dynamics of land use in the context of current conservation policies and land tenure in the Cerrado—MA-TOPIBA region (Brazil). *Land Use Policy* **2021**, *109*, 105713. [CrossRef]
16. Parreiras, T.C.; Bolfe, É.L.; Pereira, P.R.M.; Souza, A.M.d.; Alves, V.F. Applications, challenges and perspectives for monitoring agricultural dynamics in the Brazilian savanna with multispectral remote sensing. *Remote Sens. Appl. Soc. Environ.* **2025**, *37*, 101448. [CrossRef]
17. Pereira, P.R.M.; Oliveira, M.M.N.d.; Bolfe, E.L.; Macarringe, L.S. Comparação da classificação do uso e cobertura da terra em imagens Landsat-8 e Sentinel-2 no Cerrado Maranhense. *Geo UERJ* **2023**, *42*, 66306. [CrossRef]
18. Scaramuzza, C.A.M.; Sano, E.E.; Adami, M.; Bolfe, E.L.; Coutinho, A.C.; Esquerdo, J.C.D.M.; Maurano, L.E.P.; Narves, I.S.; Oliveira Filho, F.J.B.d.; Rosa, R. Land-use and land-cover mapping of the Brazilian Cerrado based mainly on Landsat-8 satellite images. *Rev. Bras. Cartogr.* **2017**, *69*, 1041–1051. [CrossRef]
19. Bolfe, É.; Victoria, D.C.; Contini, E.; Bayma-Silva, G.; Spinelli-Araujo, L.; Gomes, D. Matopiba em crescimento agrícola: Aspectos territoriais e socioeconômicos. *Rev. Polít. Agríc.* **2016**, *25*, 38–62.
20. Brito, A.d. Heterogeneidade Espaço-Temporal do Desmatamento do Cerrado Brasileiro: Estimativas e Cenários de Emissões de Carbono. Ph.D. Thesis, Instituto Nacional de Pesquisas Espaciais, São José dos Campos, Brazil, 2016.
21. Ferreira, A.J.A. Políticas Territoriais e a Reorganização do Espaço Maranhense. Ph.D. Thesis, Universidade de São Paulo, São Paulo, Brazil, 2008.
22. Santos, M.M.; Machado, I.E.S.; Carvalho, E.V.; Viola, M.R.; Giongo, M. Estimativa de parâmetros florestais em área de cerrado a partir de imagens do sensor Landsat 8. *Floresta* **2017**, *47*, 75–84. [CrossRef]
23. Bayma-Silva, G.; Vicente, L.E.; Spinelli-Araujo, L.; Victoria, D.C.; Gomes, D.; Torresan, F.E. Dinâmica do uso e cobertura da terra na mesorregião Sul Maranhense. In *Anais do 17º Simpósio Brasileiro de Sensoriamento Remoto*; INPE: São José dos Campos, Brazil, 2015.
24. Ferreira, D.M. Mudanças de uso e Cobertura da Terra na Bacia do rio Lajeado, Estado do Maranhão. Master's Thesis, Universidade Federal do Maranhão, Balsas, Brazil, 2020.
25. Castilho, R.; Botelho, A.C.; Busca, M.D. Le secteur agroalimentaire mondialisée à Matopiba Maranhense: Analyse de la spécialisation régionale de la production de soja. *Espaço Econ.* **2021**, *21*, 1–19. [CrossRef]
26. Alves, V.E.L. Mobilização e Modernização nos Cerrados Piauienses: Formação Territorial no Império do Agronegócio. Ph.D. Thesis, Universidade de São Paulo, São Paulo, Brazil, 2006.
27. Sodré, R.B. O Maranhão Agrário: Dinâmicas e Conflitos Territoriais. Master's Thesis, Universidade Estadual do Maranhão, São Luís, Brazil, 2017.
28. Cunha, R.C.C. Gênese e Dinâmica da Cadeia Produtiva da soja no sul do Maranhão. Master's Thesis, Universidade Federal de Santa Catarina, Florianópolis, Brazil, 2015.
29. Instituto Nacional de Pesquisas Espaciais. PRODES-Incremento Anual de Área Desmatada no Cerrado Brasileiro. Available online: http://www.obt.inpe.br/cerrado (accessed on 13 January 2023).
30. Instituto Brasileiro de Geografia e Estatística (IBGE). Município de Balsas. Available online: https://cidades.ibge.gov.br/brasil/ma/balsas (accessed on 25 November 2021).
31. Silva, F.d.; Bacani, V.M. Detecção de mudanças e modelagem preditiva do uso da terra e da cobertura vegetal do Pantanal de Aquidauana-MS. *Geousp-Espaço e Tempo* **2018**, *22*, 437–456. [CrossRef]
32. Macedo, R.C.; Almeida, C.M.; Santos, J.R. Modelagem dinâmica espacial da expansão da agricultura em Campos Novos-SC. *Geosul* **2018**, *33*, 260–285. [CrossRef]
33. Sano, E.E.; Rodrigues, A.A.; Martins, E.S.; Bettiol, G.M.; Bustamante, M.M.C.; Bezerra, A.S.; Couto, A.F., Jr.; Vasconcelos, V.; Schüler, J.; Bolfe, E.L. Cerrado Ecoregions: A Spatial Framework to Assess and Prioritize Brazilian Savanna Environmental Diversity for Conservation. *J. Environ. Manag.* **2019**, *232*, 818–828. [CrossRef]
34. Ministério do Meio Ambiente. Áreas Especiais. Available online: http://mapas.mma.gov.br/i3geo/datadownload.htm (accessed on 12 January 2022).
35. Dantas, M.E.; Shinzato, E.; Bandeira, I.C.N.; Renk, J.F.C. Compartimentação geomorfológica. In *Geodiversidade do Estado do Maranhão*; Bandeira, I.C.N., Ed.; CPRM: Teresina, Brazil, 2013; pp. 1–294.
36. Garcês Júnior, A.R. Variabilidade da Chuva e Desastres Associados à Dinâmica Hidroclimática no Estado do Maranhão. Ph.D. Thesis, Universidade Federal do Ceará, Fortaleza, Brazil, 2022.
37. Blaschke, T. Object-Based Image Analysis for Remote Sensing. *ISPRS J. Photogramm. Remote Sens.* **2010**, *65*, 2–16. [CrossRef]
38. Arcoverde, G.F.B. Modelagem Dinâmica Espacial da Expansão da Área de Cana-de-açúcar: Quirinópolis (GO). Ph.D. Thesis, Instituto Nacional de Pesquisas Espaciais, São José dos Campos, Brazil, 2014.
39. Girma, R.; Fürst, C.; Moges, A. Land Use Land Cover Change Modeling by Integrating Artificial-Neural-Network with Cellular Automata-Markov Chain Model in Gidabo River Basin, Main Ethiopian Rift. *Environ. Chall.* **2022**, *6*, 100419. [CrossRef]

40. Silva, T.R.; Silva, T.R.; Sano, E.E.; Vieira, D.L.M. Mapping the regeneration potential of native vegetation in cultivated pastures of the Brazilian Cerrado. *Environ. Monit. Assess.* **2023**, *195*, 1038. [CrossRef]
41. Rouse, J.W.; Haas, R.H.; Schell, J.A.; Deering, D.W. Monitoring vegetation systems in the Great Plains with ERTS (Earth Resources Technology Satellite). In Proceedings of the 3rd Earth Resources Technology Satellite Symposium, Greenbelt, MD, USA, 10–14 December 1973; SP-351. pp. 309–317.
42. Huete, A.; Didan, K.; Miura, T.; Rodriguez, E.P.; Gao, X.; Ferreira, L.G. Overview of the radiometric and biophysical performance of the MODIS vegetation indices. *Remote Sens. Environ.* **2002**, *83*, 195–213. [CrossRef]
43. McFeeters, S.K. The use of the Normalized Difference Water Index (NDWI) in the delineation of open water features. *Int. J. Remote Sens.* **1996**, *17*, 1425–1432. [CrossRef]
44. Zha, Y.; Gao, J.; Ni, S. Use of normalized difference built-up index in automatically mapping urban areas from TM imagery. *Int. J. Remote Sens.* **2003**, *24*, 583–594. [CrossRef]
45. Gonzalez, R.C.; Woods, R.E. *Processamento Digital de Imagens*, 3rd ed.; Pearson Prentice Hall: São Paulo, Brazil, 2010.
46. Baatz, M.; Schäpe, A. Multiresolution segmentation: An optimization approach for high quality multi-scale image segmentation. In Proceedings of the Angewandte Geographische Informations Verarbeitung XII; AGIT: Salzburg, Austria, 2000; pp. 12–23.
47. Breiman, L. Random Forest. *Mach. Learn.* **2001**, *45*, 5–32. [CrossRef]
48. Lu, D.; Weng, Q. A survey of image classification methods and techniques for improving classification performance. *Int. J. Remote Sens.* **2007**, *28*, 823–870. [CrossRef]
49. Maxwell, A.E.; Warner, T.A.; Fang, F. Implementation of machine-learning classification in remote sensing: An applied review. *Int. J. Remote Sens.* **2019**, *39*, 2784–2817. [CrossRef]
50. Melville, B.; Lucieer, A.; Aryal, J. Object-based random forest classification of Landsat ETM+ and WorldView-2 satellite imagery for mapping lowland native grassland communities in Tasmania, Australia. *Int. J. Appl. Earth Obs. Geoinf.* **2018**, *66*, 46–55. [CrossRef]
51. Mishra, P.K.; Rai, A.; Rai, S.C. Land use and land cover change detection using geospatial techniques in the Sikkim Himalaya, India. *Egypt. J. Remote Sens. Space Sci.* **2020**, *23*, 133–143. [CrossRef]
52. Andrade, M.P.d.; Ribeiro, C.B.d.M.; Lima, R.N.d.S. Modelagem dinâmica da mudança do uso e cobertura do solo na bacia hidrográfica do Rio Paraíba do Sul a partir de imagens Modis e um modelo de sub-regiões. *Rev. Bras. Cartogr.* **2016**, *68/6*, 965–978. [CrossRef]
53. Landis, J.R.; Koch, G.G. The Measurement of Observer Agreement for Categorical Data. *Biometrics* **1977**, *33*, 159–174. [CrossRef]
54. Aguiar, A.S. Modelagem da Dinâmica do Desmatamento na Região do MATOPIBA até 2050. Master's Thesis, Universidade de Brasília, Brasília, Brazil, 2016.
55. Campos, P.B.R. Modelo de Autômato Celular Aplicado no Estudo da Influência dos Centros Educacionais Unificados na Dinâmica de Transição do Uso e Ocupação do Solo da Periferia de São Paulo. Ph.D. Thesis, Universidade de São Paulo, São Paulo, Brazil, 2018.
56. Coe, M.T.; Costa, M.H.; Soares-Filho, B.S. The influence of historical and potential future deforestation on the stream flow of the Amazon River—Land surface processes and atmospheric feedbacks. *J. Hydrol.* **2009**, *369*, 165–174. [CrossRef]
57. Salmona, Y.B. Cerrado com C ou com S? Modelagem de Cenários Futuros para o Bioma. Master's Thesis, Universidade de Brasília, Brasília, Brazil, 2013.
58. Lima, T.C. Modelagem dos Vetores de Mudança na Paisagem no Bioma Cerrado. Master's Thesis, Universidade Federal de Minas Gerais, Belo Horizonte, Brazil, 2013.
59. Bolfe, É.L.; Victoria, D.d.C.; Sano, E.E.; Bayma, G.; Massruhá, S.M.F.S.; de Oliveira, A.F. Potential for Agricultural Expansion in Degraded Pasture Lands in Brazil Based on Geospatial Databases. *Land* **2024**, *13*, 200. [CrossRef]
60. Pimenta, F.M.; Rudorff, B.F.T.; Aguiar, D.A.; Adami, M.; Giarolla, A.; Carneiro, F.M. Historical Changes in Land Use and Suitability for Future Agriculture Expansion in Western Bahia, Brazil. *Remote Sens.* **2021**, *13*, 1088. [CrossRef]
61. Stein, B. Insights on the Potential of Natural Regeneration to Restore Cerrado Open Ecosystems. *Austral Ecol.* **2025**, *50*, 123–137. [CrossRef]
62. Santos, G.L.; Almeida, R.C.; Oliveira, P.M. Natural Regeneration in Anthropogenic Environments Due to Agricultural Use in the Cerrado, Uberaba, MG, Brazil. *Biosci. J.* **2017**, *33*, 987–998. [CrossRef]
63. MapBiomas Project. Collection 7.0 and 8.0 of Brazilian Land Cover and Land Use Map Series. Available online: https://brasil.mapbiomas.org/en/ (accessed on 20 October 2025).
64. Obaid, A.; Adam, E.; Ali, K.A. Land use and land cover change in the Vaal Dam catchment, South Africa: A study based on remote sensing and time series analysis. *Geomatics* **2023**, *3*, 205–220. [CrossRef]
65. Millogo, A.M.D.; Tankoano, B.; Neya, O.; Folega, F.; Wala, K.; Hackman, K.O.; Namoano, B.; Batawila, K. Spatiotemporal analysis of land use and land cover dynamics of Dinderesso and Peni forests in Burkina Faso. *Geomatics* **2024**, *4*, 362–381. [CrossRef]

66. Gong, P.; Liu, H.; Zhang, M.; Li, C.; Wang, J.; Huang, H.; Clinton, N.; Ji, L.; Li, W.; Bai, Y.; et al. Stable Classification with Limited Sample: Transferring a 30-m Resolution Sample Set Collected in 2015 to Mapping 10-m Resolution Global Land Cover in 2017. *Sci. Bull.* **2019**, *64*, 370–373. [CrossRef]
67. Souza, C.M., Jr.; Shimbo, J.Z.; Rosa, M.R.; Parente, L.L.; Alencar, A.; Rudorff, B.F.T.; Hasenack, H.; Matsumoto, M.; Ferreira, L.G.; Souza-Filho, P.W.M.; et al. Reconstructing three decades of land use and land cover changes in Brazilian biomes with Landsat archive and Earth Engine. *Remote Sens.* **2020**, *12*, 2735. [CrossRef]
68. Rau, M.F.N.; Calamari, N.C.; Mosciaro, M.J. Dynamics of past forest cover changes and future scenarios with implications for soil degradation in Misiones rainforest, Argentina. *J. Nat. Conserv.* **2023**, *73*, 126391. [CrossRef]
69. Câmara dos Deputados. Projeto de Lei nº 364/2019. Available online: https://www.camara.leg.br/proposicoesWeb/fichadetramitacao?idProposicao=2190986 (accessed on 12 October 2025).
70. Ministério da Agricultura, Pecuária e Abastecimento (MAPA). *Programa Nacional de Conversão de Pastagens Degradadas em Sistemas de Produção Agropecuários e Florestais Sustentáveis (PNCD)*; MAPA: Brasília, Brazil, 2020. Available online: https://www.planalto.gov.br/ccivil_03/_ato2023-2026/2023/decreto/d11815.htm (accessed on 20 October 2025).